Marine Geology 477 (2024) 107407



Contents lists available at ScienceDirect

Marine Geology

journal homepage: www.elsevier.com/locate/margo

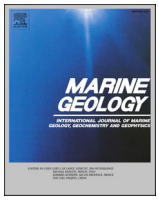

Research Article



# Sedimentological evidence of Late Pleistocene Shorelines in Oman

V. Decker [a,*], M. Falkenroth [b], G. Hoffmann [a,c]

[a] RWTH Aachen University, 52056 Aachen, Germany
[b] TU Darmstadt, 64287 Darmstadt, Germany
[c] German Commission for UNESCO, Global Geoparks Unit, 53175 Bonn, Germany

ARTICLE INFO

Editor: Edward Anthony

*Keywords:*
Last interglacial shorelines
Sea-level change
Beach processes
Foraminifera
Oman
Indian Ocean

ABSTRACT

As the climate crisis intensifies, estimating sea-level rise will become increasingly relevant, in particular assessing changes in the relative sea level in different regions. One key to comprehending global sea-level changes is the study of past sea-level highstands. Many regional studies help refine the reconstruction of paleo sea levels globally. Thus far, the Middle East remains understudied.

This paper presents evidence for Quaternary sea-level variations along the shores of the western Indian Ocean. Eight coastal outcrops along the northern and eastern coasts of Oman are presented in detail. The sedimentological evidence for sea-level highstands varies within the study area. However, in relation to recent sea-level conditions, all of these marine and beach deposits are now found well above the environments where such formations would typically form. Dating the timing of sea-level highstands remains a challenging task within the study area. In different studies, attempts to $^{14}C$ date samples from that area were unsuccessful, as the time of sediment deposition lies beyond the dating limit of $^{14}C$, precluding a Holocene formation of these sediments. Thus, the sediments are regarded as deposits formed during Pleistocene sea-level highstands, presumably during MIS 5e. For some sections, optically stimulated luminescence dating could provide a solution, as igneous source rocks supply quartz and feldspar. This paper aims to localise eight sea-level related outcrops along the Omani coast and depict their potential for future work, which should include dating and elevation measurements. Through this, our work contributes to the ongoing effort to globally identify records of sea-level changes, as well as providing insights into the regional setting in Oman.

## 1. Introduction

Coastal zones have always been attractive for humans to settle (Erlandson, 2017; Small and Nicholls, 2003). This is due to the accessibility to freshwater and seafood, as well as the advantages for trade routes and eventually their attractiveness as sites for industries. Today, 75 % of the megacities are located directly at the coast (Bange et al., 2017). Concurrently, these areas are facing mounting challenges, chiefly due to the anthropogenic climate change causing global sea levels to rise at an unprecedented pace compared to the late Holocene (IPCC, 2023; Haigh et al., 2014; McGranahan et al., 2007). This is particularly relevant in that human societies evolved during a period of relative climate stability, where sea levels remained comparatively stable for an extended period (Steffen and Wu, 2011). A sea-level rise of 3.6 mm per year was observed during the period 1993–2015 (Oppenheimer et al., 2019) which threatens millions of people and leads to huge logistical challenges regarding humanitarian and economic aspects.

The study of Quaternary sea-level fluctuations is crucial for understanding the impact of recent sea-level changes. The main mechanisms behind Quaternary eustatic sea-level variations, which depict the global oscillations, are driven by changes in Earth's orbit, which affect insolation, leading to glaciation and melting of terrestrial-based ice masses (e.g., Rovere et al., 2016a, 2016b; Paillard, 2010; Church et al., 2001; Imbrie et al., 1984; Imbrie and Imbrie, 1980; Milankovitch, 1941). One important factor related to Quaternary sea-level changes is Glacial Isostatic Adjustment (GIA) (Peltier, 1999). This describes the post-glacial rebound of the Earth's crust when the ice mass on top of it is reduced, as well as all other associated processes (Li et al., 2023; Spada, 2017). The GIA affects sea levels worldwide (Mitrovica and Milne, 2002; Mitrovica and Peltier, 1991), even well beyond the time after glaciers have melted (Spada, 2017). The spatio-temporal variability of the mantle's response to deglaciation processes varies significantly and non-overlapping sea-level highstands may belong to a single deglaciation process. Therefore, it is advisable to consider site-specific signals of

* Corresponding author.
*E-mail address:* valeska.decker@rwth-aachen.de (V. Decker).

https://doi.org/10.1016/j.margeo.2024.107407
Received 9 January 2024; Received in revised form 22 September 2024; Accepted 27 September 2024
Available online 30 September 2024
0025-3227/© 2024 The Authors. Published by Elsevier B.V. This is an open access article under the CC BY license (http://creativecommons.org/licenses/by/4.0/).

relative sea level (rsl) (Lambeck et al., 2002).

In addition to these global processes, regional factors such as subsidence and uplift, sediment influx and compaction also apply. Thus, the site-specific rsl is the one that provides a real, measurable sea-level elevation at a specific location (Rovere et al., 2016b).

Past interglacial periods are highly relevant, as they enable the study of climate systems and sea-level conditions during times as warm as or slightly warmer than today (Rohling et al., 2019; Rovere et al., 2016a; Pedoja et al., 2014). The study of Pleistocene shorelines is essential to understand the fundamental processes in coastal geomorphology and coastal groundwater dynamics related to sea-level rise. The Last Interglacial (Marine Isotope Stage (MIS) 5e; 129–116 ka,e.g., Barlow et al. (2018), is of particular interest as it is one of the closest climatic analogues to the Holocene. During this period, the global mean surface temperature was 0.5–1.0 °C warmer as well as the global mean sea level (msl) was higher than today (Oppenheimer et al., 2019). How much higher it was is still under debate. Recent studies have reached a consensus of a MIS 5e sea level peaking around 1–5 m higher than present mean sea level (pmsl) (Dumitru et al., 2023; Dyer et al., 2021), whereas previous studies reconstructed sea-level highstands of up to 9 m during MIS 5e (e.g. Dutton and Lambeck, 2012). Insights from the study of sea-level variability during this period hold the potential to significantly enhance our understanding of future changes (Deiana et al., 2021). However, paleo-shorelines are the result of the interaction between eustatic changes and local isostatic, neotectonic and erosional processes (e.g. De Santis et al., 2023; Cerrone et al., 2021a, 2021b; Chauveau et al., 2021; De Giosa et al., 2019; Milne and Mitrovica, 2008; Lajoie, 1986). Local studies addressing the interaction of these forcings and processes provide a better understanding of coastal stratigraphies and rsl changes (e.g. Chauveau et al., 2024a; Pedoja et al., 2014).

The Middle East is of particular interest for past sea-level reconstructions because this area is located at a certain distance to the Pleistocene iceshields: it lies between the so-called near-field and far-field locations (Yokoyama and Purcell, 2021), where near-field locations are in direct proximity to the limits of Pleistocene ice sheets. However, in order to understand and model the glacio-hydro-isostatic adjustment, sea-level studies in far-field locations and intermediate areas are needed (Milne, 2009). Despite recent research efforts along the coastline of Oman (Hoffmann et al., 2020a; Ermertz et al., 2019; Falkenroth et al., 2019; Moraetis et al., 2018), little is known about the remains of past interglacial shorelines along the Indian Ocean's coastline of the Arabian Peninsula (Rovere et al., 2023). Thus, the broader picture remains elusive. This is in part due to a lack of suitable sea-level archives. Consequently, research on Arabian paleo sea level is challenging and often relies only on geomorphological evidence and limited outcrops that show marine or beach deposits. In addition to these challenges, the use of sea-level index points following the guidelines of Hijma et al. (2015) is outstanding in this region. These index points serve as crucial reference markers for reconstructing past sea levels and understanding the region's geological history. The guidelines provide a protocol for standardized field survey and sample investigation to create a sea-level database. The main advantage of these guidelines is the comparability with other findings worldwide and throughout different timescales (Hijma et al., 2015).

Another compelling incentive for studying sea-level changes lies in their relevance to archaeological issues. Potential migration routes of early human populations can be reconstructed based on ancient coastline configurations (Petraglia et al., 2015; Rose et al., 2011).

Here, we present sedimentological evidence for a significant sea-level highstand, most likely related to the Last Interglacial period along the coastline of Oman. The focus of this paper is the identification and documentation of locations in Oman where Pleistocene sea-level can be studied. This work can, therefore, provide a basis for future studies and modelling work.

## 2. Study area

### 2.1. Regional setting

Oman is situated in the eastern part of the Arabian Peninsula, with its coastline bordered by the Gulf of Oman to the north and the Arabian Sea to the east, both of which are part of the Indian Ocean (Fig. 1). Along its entire coastline, there is a narrow continental shelf, leading to a seamless

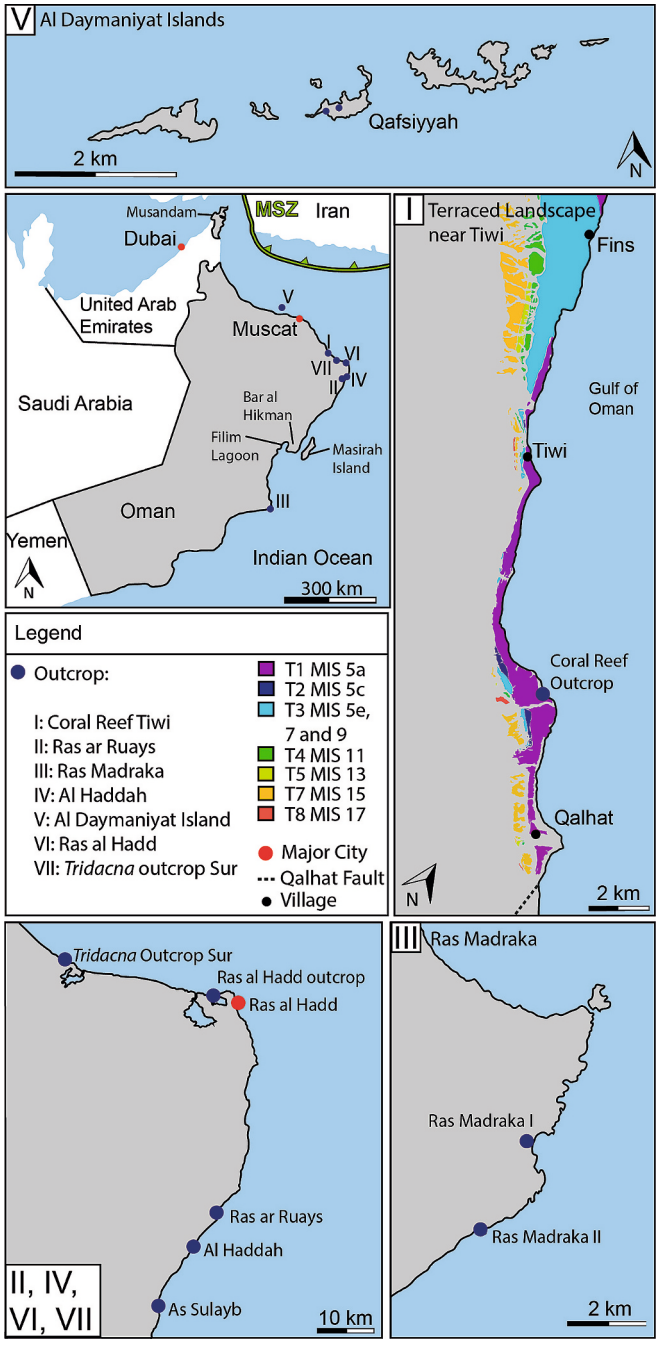


**Fig. 1.** Overview map of the study area in Oman. Major cities in this region are marked with a red dot, all eight outcrops with a blue dot. The upper map displays the location of outcrop V, Qafsiyya within the Daymaniyat Islands. The right map indicates the location of the coral reef near Tiwi and highlights the outcrop's position within the colourful marked marine terraces setting, which range in this section from ca. 15 m above pmsl (T1, purple) to ca. 250 m above pmsl (T8, orange). (For interpretation of the references to colour in this figure legend, the reader is referred to the web version of this article.)

transition from the shoreline to the deep sea. The Omani coastline, including the Musandam enclave and Masirah Island, spans over 2300 km. Approximately 1200 km of Oman's coastline consists of sandy beaches (McLachlan et al., 1998), while some tidal flats can be found in sheltered lagoons, such as in Sur, or in embayments, like the area west of Bar al Hikman (Fig. 1). These low-energy environments alternate with rocky shores, including steep cliffs in the northern region, such as those north of Ras ar Ru'ays. The entire eastern coast is exposed to the Indian Ocean with a mean swell of 0.4–0.8 m, however, with a frequency of less than 10 % waves can reach heights of up to 2 m (Sana et al., 2023). The study area is situated along the northern and eastern coastlines of Oman. The tide regime is mesotidal, with spring tides reaching up to 3 m in height. Wave energies are generally low to moderate (McLachlan et al., 1998) with mean wave heights of 0–0.8 m for this coast (Sana et al., 2023).

The northern Omani coast is dominated by the alluvial plain of the Hajar Mountains. The coastline here is flat and experiences mostly low wave energy due to the relatively narrow Gulf of Oman. However, despite its low energy, this coast is susceptible to tsunamis and has been impacted by several tsunami events over time: A severe tsunami hit the coastline ~1000 years ago (Decker et al., 2022; Hoffmann et al., 2020b) and several smaller tsunami waves reached the Omani coast in recent history. Most notably are the ones 1945, 2010 and 2013 with wave heights of less than 3 m (Hoffmann et al., 2013). This tsunamigenic potential is attributed to activities in the Makran Subduction Zone (MSZ), which runs semi-parallel to the coast northeast of Oman (Kukowski et al., 2000). Tsunamis can also be triggered or exacerbated by submarine slides within the Gulf of Oman (Heidarzadeh and Satake, 2017; Hoffmann et al., 2013).

The distal parts of the large alluvial fans that stretch along the northern coast are composed of sediments originating from the massive mountain chain located 30 km to the south. The Hajar Mountains consist mainly of highly karstified limestone, reaching heights of up to 3000 m and spanning over 600 km from Musandam in the northwest to Ras al Hadd in the east. Eastward, the alluvial fans disappear and autochthonous Eocene limestone forms the coastal area. Near Fins and Tiwi, wave-cut platforms are carved into this limestone (Fig. 1-I). Nine marine terraces were extensively described by Hoffmann et al. (2020a) who postulate that each terrace represents a Pleistocene sea-level highstand, ranging from MIS 5a to MIS 19 (82 to 790 ka). The various levels illustrate uplift in this area with different uplift rates varying in space and time from near zero in the northern part up to 0.85 mm per year in the southeast part of the marine staircase (Hoffmann et al., 2020a). This distinctive landform terminates to the southeast with the Qalhat fault, near Sur (Fig. 1I) (Ermertz et al., 2019). Several mangrove-fringed lagoons can be found between Sur and Ras al Hadd. Heading southward, the shoreline is predominantly characterized by semi-consolidated and active dunes as well as sabkha environments, characterized by their shallow basins without surface drainage meaning that they become temporarily water-filled after heavy rainfalls or spring tides (Al-Farraj, 2005). This shift in the environment is a result of a different geomorphological setting without uplift and without the direct influence of erosional processes and gravel deposits of the Hajar Mountains on one hand (Béchennec et al., 1993). On the other hand, a different rain pattern with fewer wet air masses lead to a more arid climate along the east coast (Enzel et al., 2015). Overall, Oman experiences a semi-arid to arid climate (Kwarteng et al., 2009). Due to steep slopes, limited soil, and sparse vegetation, rainfall often leads to significant surface runoff resulting in wadi flash floods with severe impact on human society as well as the environment (Saber et al., 2022). The rain shadow area to the south of the Hajar mountain chain is characterized by sand desert environments. Quaternary climate changes in the region have been reconstructed using various proxies (Decker et al., 2021; Engel et al., 2017; Enzel et al., 2015, Enzel et al., 2017; Lézine et al., 2002, 2017; Burns et al., 2001).

### 2.2. Regional Quaternary sea-level studies

Evidence of Quaternary sea-level fluctuations has been established in Saudi Arabia by Dullo (1990). He investigated terraces all along the Saudi Arabian coastline focussing on paleo reef facies. Three reef units were detected forming these steps and they were sampled for dating. U/Th-dating clustered ages of 86–118 ka for the lower reef unit and approximately 205 ka for the middle one which Dullo (1990) associates with sea-level highstands. The dating of the upper reef unit failed; the age is assumed to be 290–340 ka which correlates with the preceding sea-level highstand. The elevations of the terraces associated with the youngest reef unit vary significantly along the coast with 1.5–12 m above pmsl and up to 20 m pmsl in the Gulf of Aqaba in the north. The terraces belonging to the middle unit reach 26–57 above pmsl. As the tectonic setting remains unclear and quantitative uplift rates are missing, this work shows sea-level fluctuation evidence but lacks information for a quantitative analysis.

At the coasts of the Gulf of Suez, 125 ka old coral terraces at ~10 m elevation above pmsl indicate a sea-level highstand within the Last Interglacial (Bosworth and Taviani, 1996). Parker et al. (2012) pin two marine terraces at elevations of 0.5 to 8 m above pmsl at the coastline of the Sinai Peninsula, in the northern Red Sea, to MIS 5 (77–129 ka). Other evidence of former sea-level highstands is preserved in the form of emerged marine terraces documented along the Makran coast of Iran and Pakistan (Normand et al., 2019; Reyss et al., 1999; Harrison, 1941). These terraces stretch along the entire Iranian and Pakistani coastline of the Gulf of Oman. According to these investigations, the Makran terraces mainly formed during MIS 3, 5 and 7 and are found at elevations of ca. 5 to 70 m above pmsl. Some undated marine terraces can be found at elevations of up to ca. 160 m above pmsl and were linked to previous highstands up to MIS 17 by Normand et al. (2019). For this coast, they postulate uplift rates varying approximately from 0.05 to 1.2 mm per year (Normand et al., 2019).

Research on Oman's coasts (Hoffmann et al., 2020a) detected a similar morphological setting of marine terraces near Fins and Tiwi at the north eastern coast. These uplifted terraces were assigned to MIS 5, 7, 9, 11, 13, 15, 17 and 19 based on an age model with cosmogenic nuclide ($^{10}$Be $^{36}$Cl) and OSL dating (Hoffmann et al., 2020a). Potential MIS 5e sea-level proxies in Oman, United Arab Emirates, Qatar and Iran are described by Falkenroth et al. (2019, 2020), Williams and Walkden (2002), Oveisi et al. (2007) and Pirazzoli et al. (2004).

Though indicating a relative sea-level highstand, uplifted marine terraces are not suitable for paleo sea-level reconstruction as uncertain uplift rates may lead to miscalculations in reconstructing sea-level elevations. Instead, paleo marine deposits in tectonically stable areas are of high value to refine the amplitude of sea-level oscillations (Pirazzoli, 1993). Tectonic stability is postulated for the study area east of the marine terraces block which is separated by the Qalhat fault (Fig. 1I) from the area around Sur (Falkenroth et al., 2020) and the northern part of the east coast (Decker et al., 2021; Hoffmann et al., 2013). Near Sur, Falkenroth et al. (2020) describe coastal notches with apexes at an elevation of 3.93 ± 0.12 m above pmsl. The elevation was measured using a Differential Global Positioning System (DGPS) and the pmsl was used as a reference point. The age model combines a maximum age that is the age of a fanglomerate that formed before the formation of the notches and a minimum age which is the age of a nearby beachrock. Cosmogenic radionuclide $^{10}$Be dating on fanglomerate quartz pebbles reveals a maximum age for the notch of 371 ± 38 ka and a previously published OSL dating on quartz grains in a nearby beachrock reveals a minimum age of 80 ± 3 ka (Mauz et al., 2015). Falkenroth et al. (2020) associate the formation of the notches around Sur to the Last Interglacial and postulate a sea-level highstand of 3.93 ± 0.12 m during MIS 5e.

Holocene sea-level research activities are more widespread due to the higher preservation potential and interdisciplinary interest, as archaeological research for example addresses broad scientific issues like landscape evolution and paleoshorelines to identify migration or

trade routes (Berger et al., 2013). In Oman, some studies (Berger et al., 2020; Berger et al., 2013; Preusser et al., 2005; Lézine et al., 2002) document records like paleolake and paleolagoonal sediments of a potential Mid- or Late-Holocene sea-level highstand, however, the assumed sea-level elevations are highly inconsistent. Berger et al. (2013) postulate a sea-level of up to 9 m above pmsl ca. 7 ka BP, 2–3 m of which are assigned to an eustatic highstand and 2–3 m of post-sedimentary effects, namely tectonic uplift. Lézine et al. (2002) postulate a 'slight seawater incursion' around 5 ka BP. Contradictorily, investigations on paleo mangrove sediments by Decker et al. (2021) precludes a Holocene sea-level highstand and finds the region to be tectonically stable, which is supported by a study on paleo coastal notches in Sur (Falkenroth et al., 2020).

## 3. Methods

### 3.1. Fieldwork and sedimentological investigation

Fieldwork was conducted in 2021, 2022 and in 2023. Eight coastal outcrops were investigated along the north and east coast of Oman (Fig. 1, Table 1). The locations are presented as meters within the Universal Transverse Mercator (UTM) projection, Zone 40Q using the WGS 1984 reference ellipsoid.

For the sedimentological facies analysis, all eight outcrops are described including grain size, sedimentological textures, structures, ichnology and fossil content of the observed layers. The indicated heights of the specific layers were determined by using a measuring tape, we defined the base of a profile as zero. The layers are then grouped into lithofacies based on their sedimentological properties. Facies associations are defined by lithofacies and facies architecture as well as stratigraphical relationship. Each outcrop is interpreted regarding its depositional realm taking also microfossil data into account.

### 3.2. Microfossil analysis

Two samples (S1 and S2) from Ras ar Ru'ays were collected for microfossil analysis. The two lowermost layers of the profile seemed especially suitable for microfossil analysis as their clay to silt grain size provides good preservation potential. To loosen the cemented sediments, they were washed and then dried in an oven at 50 °C. Material smaller than 0.063 mm was removed by wet sieving. Afterwards, the foraminifera were extracted by using a microscope.

Quantity, species assemblage, biodiversity and relative abundance of the three different foraminiferid test types are indicative for specific environmental conditions (Murray, 1991; Brasier, 1980). Eutrophic conditions and biodiversity are determined by the relationship of quantity and number of species, this is displayed in the Fisher-α-index. The Shannon-Weaver-index (*H*) is a measure for species diversity within a given ecosystem. It is calculated by the total amount of each species, the proportion each species is out of the sum of specimen, and sums the proportion multiplied by the natural log of that proportion. The Shannon-Weaver index provides a single value that reflects both the number of different species present (species richness) and their relative abundances (species evenness) within the ecosystem. Higher values of the index indicate greater species diversity, while lower values indicate lower diversity. It is a useful tool in ecology and conservation biology for comparing the diversity of different ecosystems and assessing the impact of environmental changes on biodiversity. Our interpretation of environmental conditions is based on the relation of the Fisher-α- and the Shannon-Weaver-indices. The different foraminiferid test types are presented in a ternary diagram. The distributional patterns can already be indicative for different milieus (Murray, 1991). Thus, foraminiferal analyses are appropriate to estimate subjects like environmental setting, salinity and wave energy and can help to complete the sedimentological description.

## 4. Observations and interpretation

Along the northeastern coastline of Oman, between Muscat in the north and Ras Madraka in the south (Fig. 1), a number of outcrops reveal marine facies occurring at elevations of approximately 1–18 m above pmsl. For a summary of all outcrops described in this study with locations, observed lithofacies and samples see Table 1. Additional data related to this article can be found at (https://data.mendeley.com/datasets/6yx52x7cvv/1), an open source online data repository hosted at Mendeley Data (Decker et al., 2024).

### 4.1. Outcrop I: Profile fossil coral reef in Tiwi

A roughly 300 m wide and 10 to 15 m high coastal cliff section 5 km south of the village Tiwi (Fig. 1) exposes fossil coral reefs. The modern beach at the foot of the cliff is a gravel beach with a steep profile, a high berm and no considerable backbeach. The cliff itself consists of two

**Table 1**
General overview of all described outcrops in this paper including name, their location with different coordinate systems, findings and sample site where applicable.

| | | location (WGS84) | | | | | | | | |
|---|---|---|---|---|---|---|---|---|---|---|
| | | Decimal degrees | | Degree/Min/Sec | | UTM-Coordinates | | | | |
| | Name Outcrop | Latitude (°N) | Longitude (°E) | Latitude (N) | Longitude (E) | Z | E | N | Observed lithofacies | Samples |
| 1 | Coral-Outcrop Tiwi | 22.751618 | 59.328755 | 22°45′5.8248" | 59°19′43.518" | 40Q | 739135.258 | 2517904.534 | Coral reef/debris flow deposits | Thin sections 30 cm + 160 cm: forams |
| 2 | Profile Ras ar Ru'ays | 22.181339 | 59.768410 | 22°8′31.6644" | 59°39′20.7432" | 40Q | 773926.700 | 2450952.744 | Tidal flat facies and fluvial deposits | |
| 3 | Profile Ras Madraka I | 18.9823096 | 57.8098511 | 18°58′56.31456" | 57°48′35.46396" | 40Q | 585247.998 | 2099066.029 | Paleobeach | |
| 4 | Profile Ras Madraka II | 18.969326 | 57.787767 | 18°58′09.5736" | 57°47′15.9612" | 40Q | 582929.647 | 2097618.775 | Paleobeach | |
| 5 | Profile Al Haddah | 22.133500 | 59.728417 | 22°08′00.6" | 59°43′42.3" | 40Q | 781441.845 | 2450129.720 | Marine facies with *Crassostrea* | |
| 6 | Daymaniyat Island Qafsiyyah | 23.855013 | 58.085087 | 23°51′18.0468" | 58°5′6.3132" | 40Q | 610493.135 | 2638597.785 | Beachrock with bioturbation and cross bedding | |
| 7 | Profile Ras al Hadd | 22.531255 | 59.760664 | 22°31′52.518" | 59°45′38.3904" | 40Q | 783962.656 | 2494254.145 | Beachrock with bioturbation | |
| 8 | *Tridacna*-outcrop Sur | 22.5878170 | 59.5081819 | 22°35′16.1412" | 59°30′29.45484" | 40Q | 757874.593 | 2500061.349 | Fossil coral reef with *Tridacna* | |

easily distinguished lithofacies that alternate one another in two cycles (Fig. 2). The reef facies is a poorly consolidated carbonate sand (facies OT1). The other facies are massive boulder fanglomerates. Due to differences in the facies' ability to withstand erosion, an up to 4 m deep overhang has developed at parts of the cliff section (facies OT2). The cliff is the seaward edge of a coastal terrace that was described in detail by Hoffmann et al. (2020a). The authors have allocated the formation of the terrace surface to a sea-level highstand at MIS 5a according to an age model developed by cosmogenic nuclide and optically luminescence dating.

#### 4.1.1. Sedimentology

Facies OT1 contains two layers of a white fine to medium gravelly sandstone that are interbedded with facies OT2. The layers stretch over the entire cliff and show no considerable variation in thickness (Fig. 2, upper part). Their surface is smoothened by erosion and displays a yellow weathering colour. The material is partially carbonate cemented. The sandstone is moderately sorted. Larger clasts, granules to cobbles, concentrate in lenses that display a shallow NW dip. All rock fragments are subrounded to well rounded, while fossils are mostly angular. Fossil debris content is high, consisting of broken gastropod and bivalve shells, sea urchins and corals. Embedded within the sandstone are in situ patch reefs and solitary corals (Fig. 2; Fig. 3 a). All corals belong to a single species within the genus *Porites* (Lars Reuning, University of Kiel, personal communication). One coral stock reaches a size of up to 1.2 m across. The individual corals are superimposed on one another and stretch over the entire thickness of the sandstone layers (up to 3 m). The material in between coral branches is poorly cemented white fine sand to silt (Fig. 3 c). It contains small, elongated, black components with uncertain origin. The material is coarsening upwards. The uppermost 0.4 to 0.5 m are enriched in echinoderm shells, coral fragments and other carbonate debris. The detected echinoderms belong to the species *Echinometra mathaei* (Fig. 3 f,g).

Facies OT2 consists of thick and massive boulder fanglomerates that are clast-supported (Fig. 3 b). Locally, lenses of matrix-supported material occur. Overall, this facies becomes more matrix rich towards the top of the profile. The matrix is coarse sand and calcite cement. The conglomerate is polymictic and very poorly sorted with clast sizes ranging from granules to boulders up to 1 m in diameter. The largest fraction of the grainsize accumulates in clusters. The clasts are subrounded limestone displaying various colours like dark grey, light grey, red or yellow. The top of the lower layer of this facies is partially encrusted by barnacles. In the lowermost part of the layer coral fragments and gastropod shells are observed (Fig. 3 d,e). Bioerosion is not evident at the clasts. The lower contact of the conglomerate layers are abrupt but conformable.

Facies OT3 consists of a few centimeter to decimetre thick layer of polymictic well-rounded pebbles and numerous mollusc shells.

#### 4.1.2. Interpretation

The presence of an in situ *Porites* reef complex in facies OT1 serves as a significant indicator of a shallow marine environment within the photic zone as the zooxanthellae-bearing animals are tied to the availability of sun light for their metabolic processes (Dullo, 2005). The growth and morphological characteristics of corals are a consequence of several influential factors (Hibbert et al., 2016). Growth rates of *Porites* depend on the species and can reach up to 36 mm/y in shallow marine environments (Dullo, 2005 and references therein). The column-like structure exhibited by these *Porites* reflects a strategic adaptation to the environmental conditions and develops only under bright light conditions (Muko et al., 2000). One of the key environmental challenges that these corals faced was the continuous influx of sediment into their

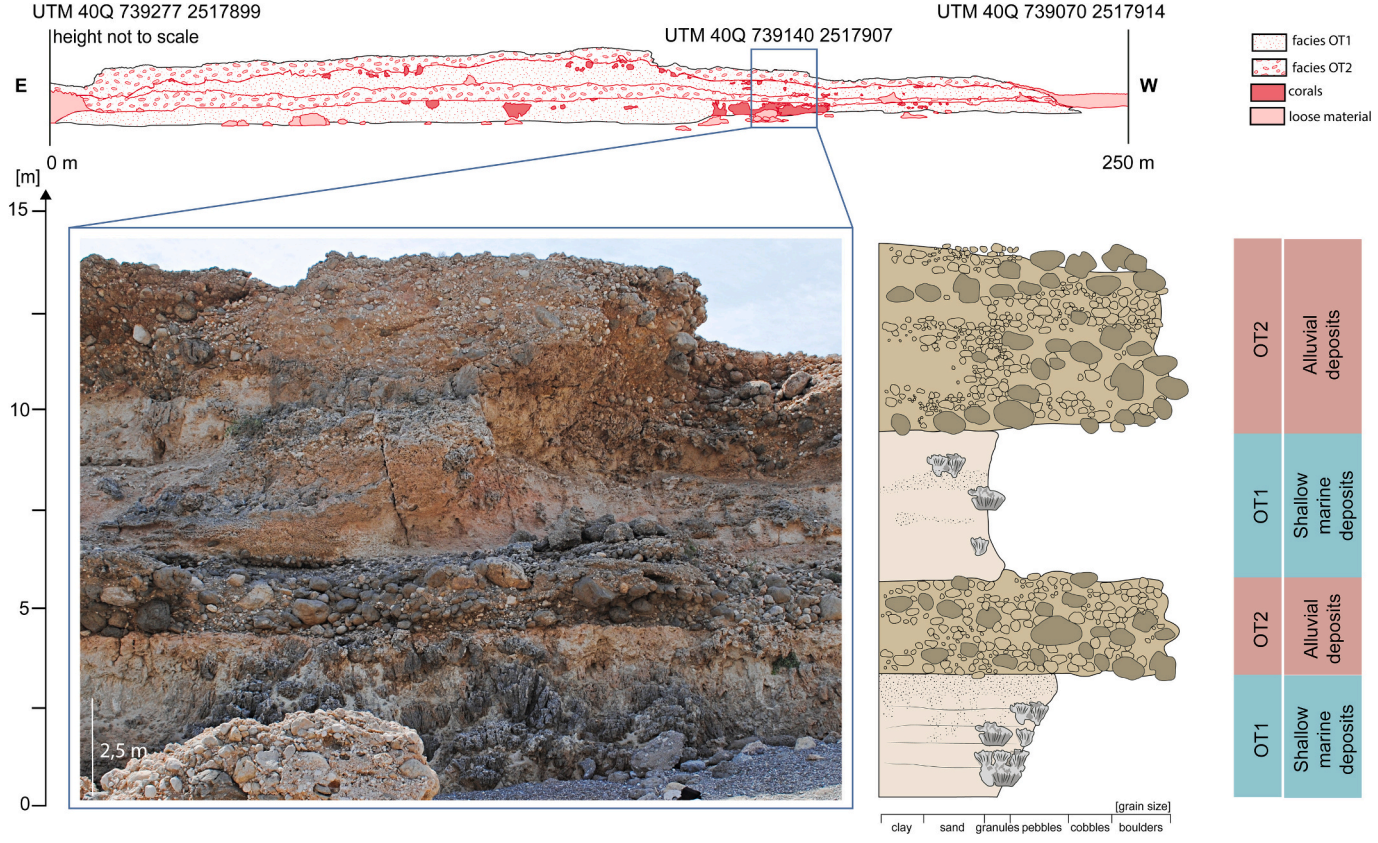


**Fig. 2.** Sketch, photo overview and a profile section of the coastal outcrop near Tiwi showing an intercalation of two cycles of an in situ coral reef and a very poorly sorted facies indicating a more terrestrial influence, most likely a debris flow within an alluvial fan. The top is an abrasional platform, and is part of the lowermost terrace of the marine terraces staircase in that area.

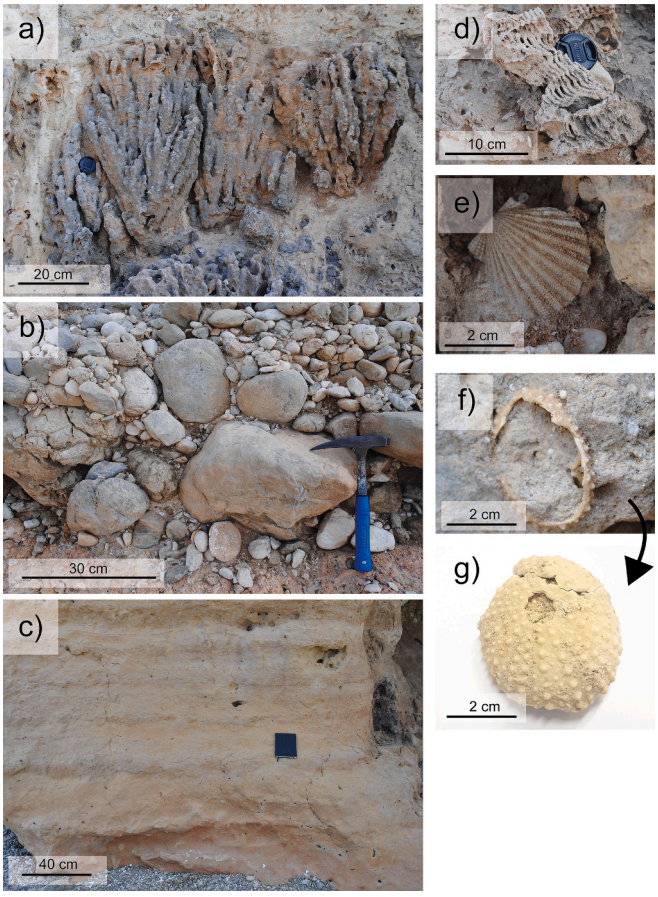


**Fig. 3.** Plate of specific features of the coastal outcrop near Tiwi, with a) facies OT1: fossil corals of a single species within the genus *Porites* (Lars Reuning, University of Kiel), the finger-like appearance of the corals reflect an adaptation to the influx of fine grain sediment that now is preserved as a light beige matrix, b) facies OT2, poorly sorted conglomerate c) fine-grained sediment, which can be found next to the patch reef and as a filling of the space between the corals (facies OT1), d) Ex situ fossil corals at the base of facies OT2, e) fossil *Pecte* bivalve shell at the base of facies OT2, f) & g) fossil echinoderm outer shell belonging to the species *Echinometra mathaei* (facies OT1).

habitat which is documented by void filling. The elongated columnar morphology of these *Porites* corals, therefore, appears to be an evolved response to mitigate the impact of sedimentation and maintain their position within the photic zone. The echinoderm *Echinometra mathaei* found in the upper part of OT1, lives in the littoral zone up to 30 m depth and is documented for the eastern Indian Ocean from the Late Pleistocene on (Philippe, 1998). The coarsening upwards of the matrix sediment indicates an ongoing change in environmental conditions.

In the geological sequence, the transition from facies OT1 to facies OT2 marks a significant shift in environmental conditions and sedimentary processes.

Facies OT2, which caps facies OT1 sharply, is characterized by distinctive characteristics like a very poor sorting and the presence of grain sizes of up to 1 m that suggest a deposition as a debris-flow with a high erosional energy. Debris flows are typically associated with terrestrial environments and are often triggered by heavy rain events or other factors that mobilize loose sediment and debris. The lack of bioerosional features support the terrestrial depositional environment. This sedimentation of facies OT2 led to the rapid burial and preservation of the underlying *Porites* reef facies OT1. Facies OT2 represents a terrestrial environment marked by periods of intense rainfall and erosional activity.

Facies OT3 depicts part of the lowermost terrace within the marine terraces stock in this area. It is an marine abrasion platform that worked up an older alluvial fanglomerate.

The alternation of a calm, shallow marine and a high energetic terrestrial facies clearly depicts an interaction of neotectonic uplift and sea-level oscillations. The marine terrace OT3 is referred by Hoffmann et al. (2020a) to a sea-level highstand at MIS 5a which gives a minimum age of 82.000 years to the sediments below. For these terraces Late Quaternary uplift rates of 0.01 to 0.89 mm, for Tiwi area 0.25–0.68 mm per year are documented by Hoffmann et al. (2020a). An ongoing recent uplift for this region is proven with uplift rates of ca. 1.3 mm per year (Pavlopoulos et al., 2023).

### 4.2. *Outcrop II: Ras ar Ru'ays*

Ras ar Ru'ays is located on the east coast of Oman (Fig. 1 II). The investigated outcrop is 6 m high and extends over ca. 280 m along the coast at the tip of Ras ar Ru'ays (Fig. 4). A total of five lithofacies are observed (OR1 to OR5). The lowermost facies OR1 and OR2 crop out at the southwestern end of the cliff and are discordantly overlain by the younger facies (Fig. 5a). While the layers of facies OR1 and OR2 are horizontal, the layers of OR3 to OR5 dip shallowly in a northwestern direction. As shown in Fig. 6, one log, comprising all observed lithofacies, is described from the southwestern section of the cliff. Furthermore, facies OR1 and OR2 were sampled for microfossil analyses.

#### 4.2.1. *Sedimentology*

Facies OR1 occurs only at a 30 m wide section at the southwestern end of the cliff and shows a total thickness of 0.2 m. It is possible that the facies continues laterally, but is not visible due to the base of the outcrop is covered by the recent beach sediment. The facies consists of greenish-grey, silty clay and is horizontally laminated. The sediment contains organic material, that shows an orange-brown oxidation colour. The organic components are pebble-sized and scattered randomly throughout the layer. No macrofossils were observed.

Sample 1 (S1) was taken within this section in an elevation of 30 cm from the profile base (Fig. 4).

Facies OR2 is a 1.7 m thick, interbedded sandy silt and pebbly fine sand. It shows a colour alternation between light greenish beige of the silt to a more reddish orange of the sand. The sediment is semi consolidated and lamination varies between strictly horizontal, wavy and convoluted. Sandy layers often display ripple lamination. Facies OR2 crops out exclusively at the southwestern end of the cliff, where it can be traced for about 80 m. Pebbles occur randomly distributed but also concentrated in layers and lenses together with coarse sand. These layers and lenses are up to few centimetres thick. The facies is inversely graded – the occurrence of pebble layers increases towards the top. The material contains macroscopic fossils of molluscs (Fig. 5b). The facies shows different degrees of bioturbation. Some layers are bioturbated by single, vertical, 0.2 to 0.6 m wide and up to 0.47 m long burrows (Fig. 5c). The burrows show a consistent thickness, no branching, no lining and are infilled by sand. In these layers the bioturbation-index (bi) is low (1 or 2) so that overall bedding boundaries remain distinct. Some sand layers display very strong bioturbation (bi = 5 to 6) that masks all individual traces. White gypsum precipitation appears on top of greenish-orange clayey fine-sandy silt.

Sample 2 (S2) was taken within this section in an elevation of 160 cm from the foot of the profile (Fig. 4).

Facies OR3 is a at least 3.4 m thick, consolidated, matrix-supported conglomerate. It displays internal bedding with decimetre thick parallel layers that dip towards the NW at a low angle. The whole facies pinches out towards the southwest, where it appears as a thin bent layer of a few centimetres. At the northeastern end of the cliff it reaches a thickness of up to 5 m. The matrix is a light beige cemented fine-sandy coarse sand. Clasts are polymictic with an especially high diversity at the base of the facies. Clasts are, with decreasing abundance: granules to

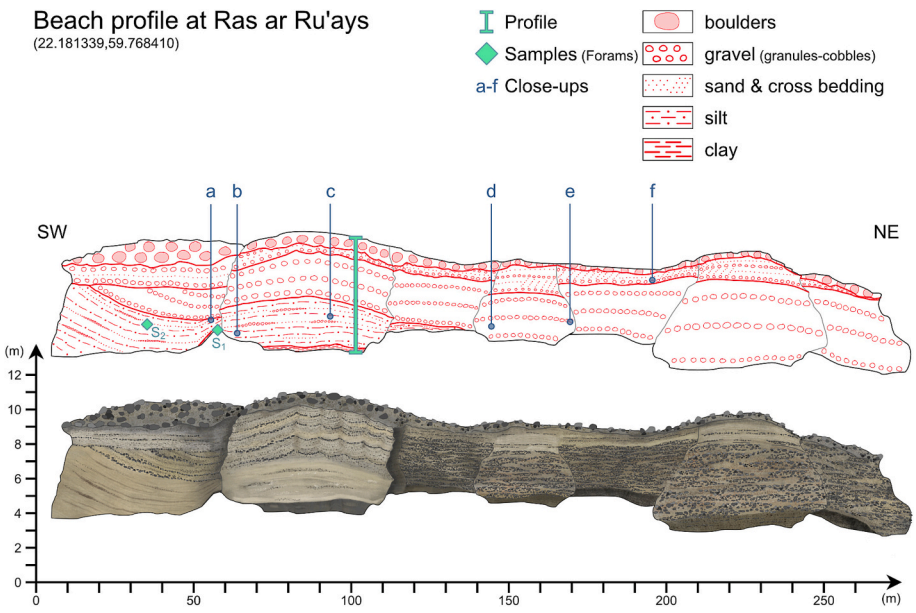


**Fig. 4.** Sketch and photo overview of the coastal outcrop near Ras ar Ru'ays, the green line indicates the location of the profile, the two green diamonds the sample locations for the foraminiferal investigation, the bluish a-f the locations of the close-up pictures in Fig. 5. (For interpretation of the references to colour in this figure legend, the reader is referred to the web version of this article.)

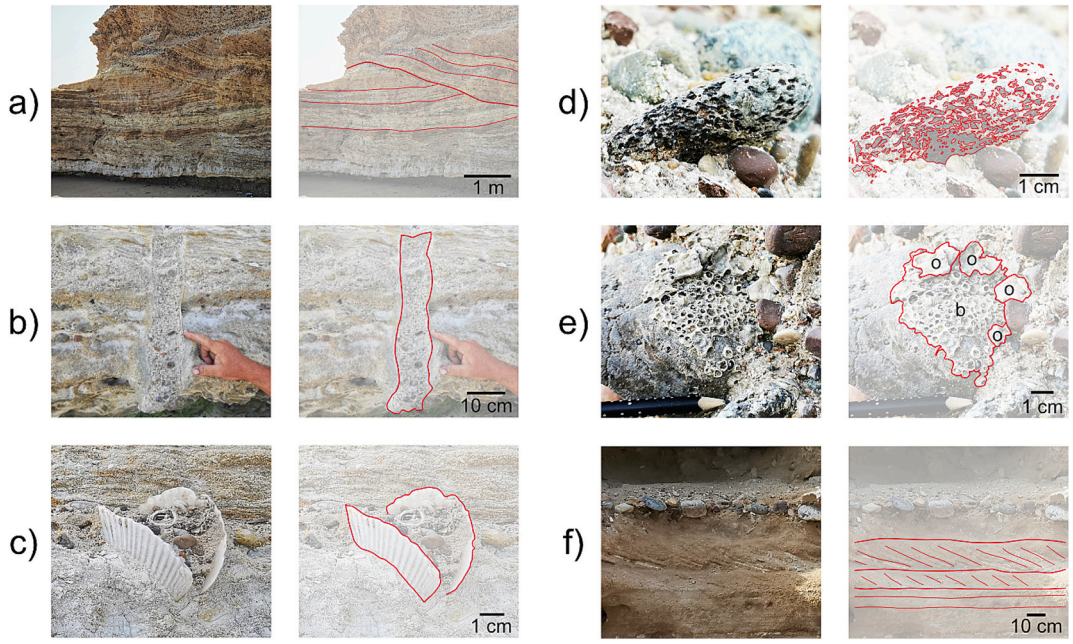


**Fig. 5.** Plate of specific features of the coastal outcrop near Ras ar Ru'ays with a) side view of the section showing cross bedding, b) bioturbation structure, filled with coarser sediment in facies OR2, c) still connected bivalve shells also in OR2, d) partly bioeroded pebble showing traces of the boring sponge *Cliona* (ichnogenus *Entobia*) that were created pre-depositional in facies OR3, e) remnants of barnacles (b) and oyster shells (o) also in OR3, f) cross bedding structures in facies OR4.

cobbles of grey, well-rounded limestones (45 %), pebbles of purple-red subrounded sandstone (20 %), pebbles of red subangular radiolarite (15 %) and pebbles of white/black rounded granite (10 %), others (10 %). Towards the top of the facies, the proportion of limestone increases significantly (up to 95 %) and replaces almost all other lithologies. The observed limestone clasts show traces of the boring sponge *Cliona* (ichnogenus *Entobia*) that were created pre-depositional (Fig. 5d). The matrix contains bivalve and gastropod shells. Additionally, some fossil oysters and barnacles are found on top of single clasts (Fig. 5e).

Facies OR4 (0.3 m thickness) shows a horizontally bedded interlayering of semi-consolidated sand and a consolidated, matrix-supported conglomerate. OR4 is similar to the base of OR3 but includes abundant reddish-beige fine-sand layers, varying in thickness of few centimetres up to ca. 0.8 m within the outcrop. Towards the northeastern part of the cliff, these sand layers partly show crossbedding structures (Fig. 5f). OR4 contains few limestone boulders up to 35 cm in diameter. The sandy layers are burrowed by vertical and oblique tubes of up to 5 cm in diameter and 15 cm in length. Some oyster shell remains can be found attached to clasts.

Facies OR5 is a 0.3 m thick, semi-consolidated, matrix-supported conglomerate. The conglomerate is polymictic with well to very well rounded limestone, granite and sandstone clasts that are mostly cobble

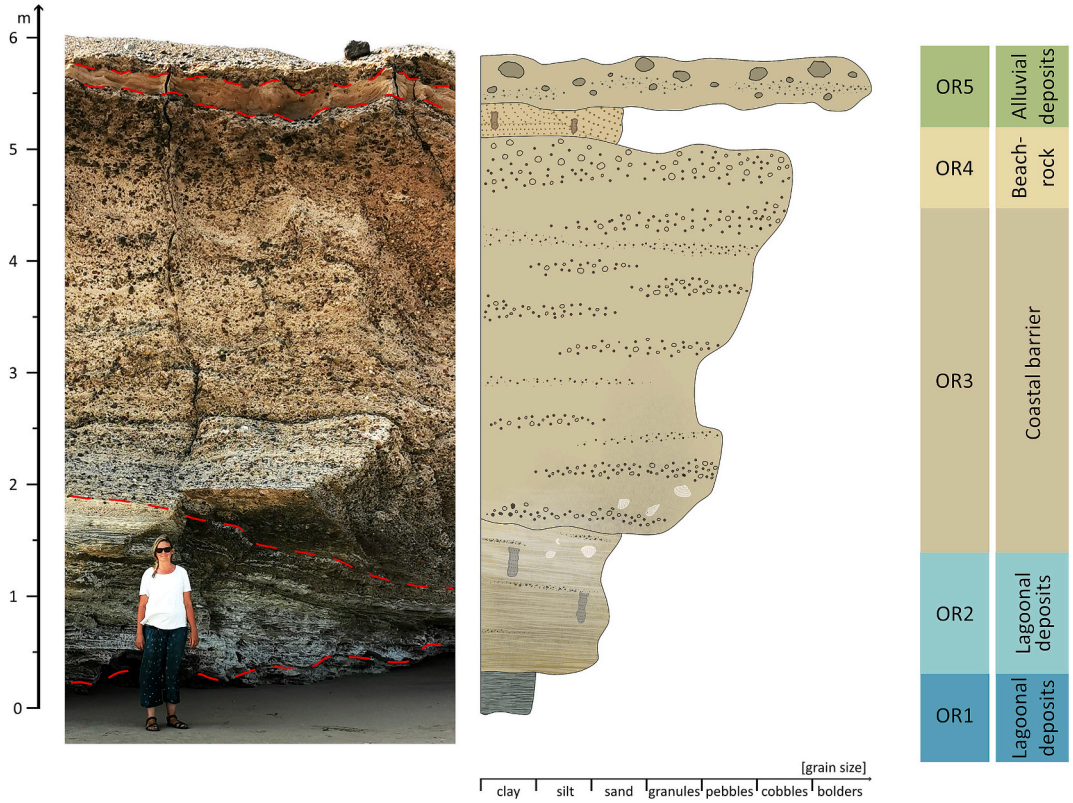


**Fig. 6.** Profile section of the coastal outcrop near Ras ar Ru'ays with the different facies ranging from marine to various terrestrial deposits.

sized. Granules, pebbles and boulders up to 35 cm in diameter also occur. The top of the layer is poorly consolidated. The matrix is light-beige.

#### 4.2.2. Microfossil analysis

In Ras ar Ru'ays two samples were taken, one at an elevation of 30 cm (S1, Facies OR1) and one at 160 cm (S2, Facies OR2) (Fig. 4).

The microscopic examination of S1 of facies OR1 depicts a low content of foraminifera. Their shells, the tests, are badly preserved and thus unsuitable for species identification.

A total of 477 individual foraminifera were separated from S2 of facies OR2; 69 of these are badly preserved and unidentifiable. Species identification was done on the remaining 408 individuals. All of these are well preserved. Even tests of fragile specimen, e.g. *Pseudononion* sp., are found complete. The 408 individuals include 20 species and 13 genera (Table 2) (Fig. 7; Fig. 8). Most of the specimen are hyaline-perforate foraminifera (Fig. 9a). Of all specimens, only three are agglutinated and two are porcelaneous, most of these are unidentifiable. The Fisher-α-index gives a value of 4.5 (Fig. 9b). The Shannon-Weaver-index amounts to 2.63 (Fig. 9c).

Additionally to foraminifera, ostracods were detected in S2. Out of all ostracods ten specimen were found with articulated valves, plus 16 single ostracod valves.

#### 4.2.3. Interpretation

At the Ras ar Ru'ays coastal site, the geological sequence distinctly reveals a transition from a marine depositional environment at the base to a more terrestrial one towards the top. A crucial aspect of reconstructing the depositional environment lies in the analysis of foraminiferal content within lithofacies OR1 and OR2 in the lowermost section.

In S1 of lithofacies OR1, the presence of foraminifera tests indicates a marine environment, although precise environmental analysis is hindered by the poor preservation of these tests in the sample. Conversely, in S2 of lithofacies OR2, foraminiferal tests are generally well-preserved, even the fragile *Pseudononion* sp. tests remain intact (Fig. 8d & e). This suggests minimal transport distance or implies that this fauna might be autochthonous.

While the position of S2 within the ternary diagram (Fig. 9a) suggests various possible environments, it does not singularly confirm the

**Table 2**
Foraminiferal species assemblage. In total 408 individuals were found, 20 different species were identified, belonging to 13 different genera.

| No. | Genera | | No. | Species | |
|---|---|---|---|---|---|
| | Name | Counted | | Name | Counted |
| 1 | *Ammonia* | 23 | 1 | cf. *Ammonia* sp. 1 | 23 |
| 2 | *Bolivina* | 15 | | *Bolivina* indiff. | 7 |
| 3 | *Cibicides* | 6 | 2 | *Bolivina* sp. 1 | 3 |
| 4 | *Elphidium* | 115 | 3 | *Bolivina* sp. 2 | 5 |
| 5 | *Lobatula* | 92 | 4 | *Cibicides refulgens* | 6 |
| 6 | *Loxostomina* | 5 | | *Elphidium* indiff. | 51 |
| 7 | *Neoconorbina* | 11 | 5 | *Elphidium* sp. 1 | 66 |
| 8 | *Operculina* | 7 | 6 | *Elphidium* sp. 2 | 14 |
| 9 | *Pararotalia* | 8 | 7 | *Elphidium* sp. 3 | 16 |
| 10 | *Procerolagena* | 1 | 8 | *Elphidium* sp. 4 | 4 |
| 11 | *Pseudononion* | 43 | 9 | *Elphidium* sp. 5 | 15 |
| 12 | *Trochulina* | 29 | | *Lobatula* indiff. | 69 |
| 13 | *Valvulina* | 2 | 10 | *Lobatula lobatula* | 14 |
| | **Total:** | **357** | 11 | cf. *Lobatula* sp. 1 | 9 |
| | | | 12 | cf. *Loxostomina* sp. 1 | 5 |
| | | | | *Neoconorbina* indiff. | 8 |
| | | | 13 | *Neoconorbina marginata* | 2 |
| | | | 14 | *Neoconorbina multimarginata* | 1 |
| | | | 15 | *Operculina* cf. *ammonoides* | 7 |
| | | | 16 | *Pararotalia* sp. 1 | 8 |
| | | | 17 | *Procerolagena* sp.1 | 1 |
| | | | 18 | cf. *Pseudononion* sp. 1 | 43 |
| | | | 19 | *Trochulina* sp. 1 | 29 |
| | | | 20 | *Valvulina* sp. 1 | 2 |
| | | | | **Total:** | **408** |

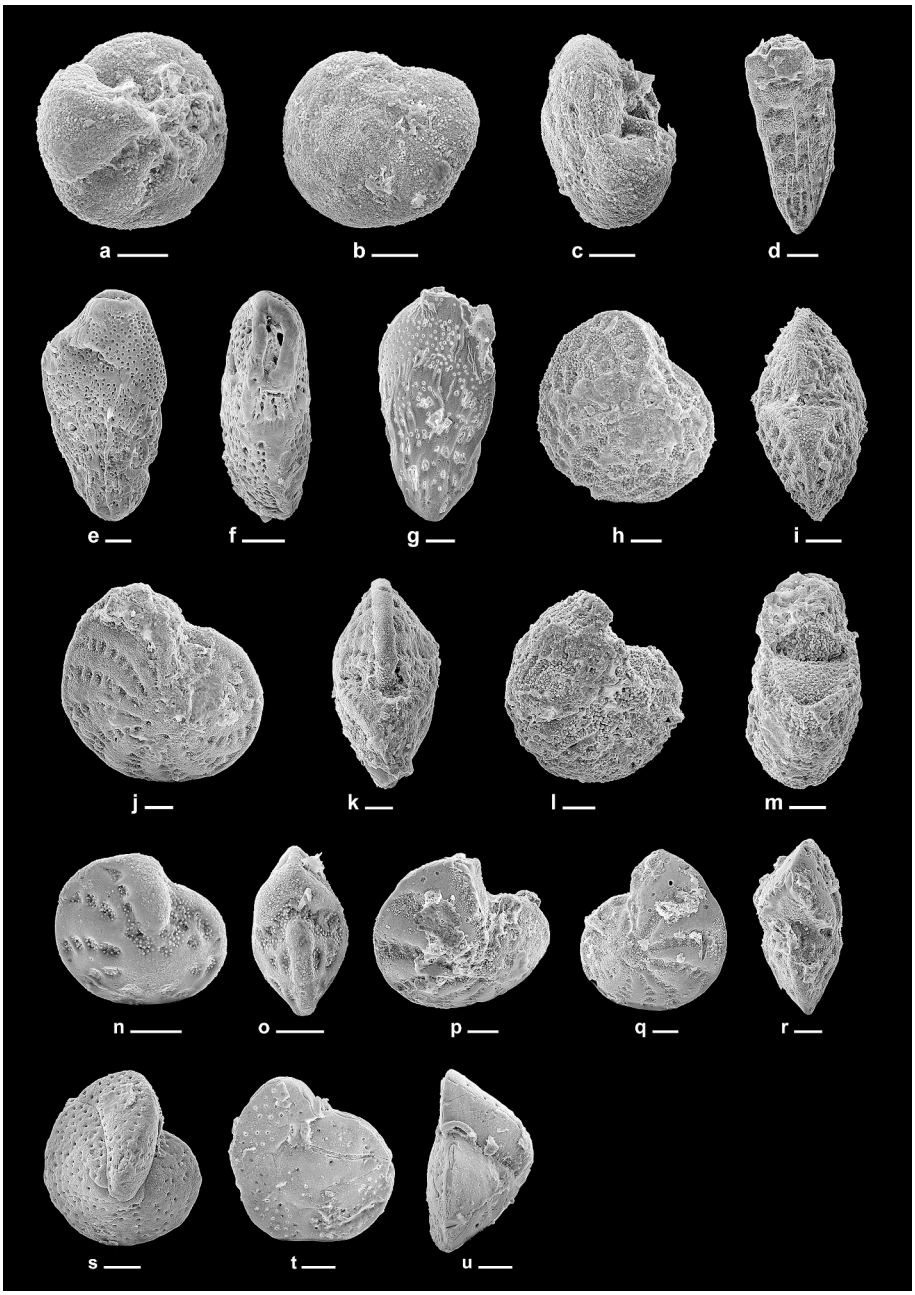


**Fig. 7.** Plate I, scale is 50 μm; a-c) cf. *Ammonia* sp. 1; d) cf. *Loxostomina* sp. 1; e,f) *Bolivina* sp. 1; g) *Bolivina* sp. 2; h,i) *Elphidium* sp. 1; j,k) *Elphidium* sp. 2; l,m) *Elphidium* sp. 3; n.o) *Elphidium* sp. 4; p-r) *Elphidium* sp. 5; s-u) *Cibicides refulgens*.

depositional background environment. The species assemblage in lithofacies OR2 includes abundant benthic and epifaunal species, like *Elphidium* sp. which preferably sits on algae, and also low-oxygen-tolerant species like *Ammonia* sp. This aligns with the deposition of fine-grained sediments resulting in low oxygen content within the sediment. The small grain size reflects a low-energy sedimentary setting while the presence of gypsum points to a shallow water body or tidal flat. This coincides with the appearance of sandy lenses and interlayers of pebbles in between which indicate the proximity to the coast.

Collectively, this sedimentary evidence paints a picture of a marine lagoon inhabited by algae and possibly mangroves, similar to today's Filim Lagoon west of Bar al Hikman. Such a specific environment is only suitable for a limited range of species. This is supported by the relatively low Fisher-α-index of 4.5 suggesting eutrophic conditions and a low biodiversity, commonly observed in muddy tidal flats rich in algae (Murray, 1991). The relationship between the Fisher-α-index and the Shannon-Weaver-index plots *Shelf* or *Normal marine to hypersaline lagoon*, the latter further supporting the lagoonal interpretation (Shannon and Weaver, 1949).

Notably absent are typical indicators of freshwater influence and typical reef indicators, with the exception of *Operculina*. The absence of larger foraminifera rules out an oligotrophic reef environment and a carbonate shelf. *Operculina* and *Pararotalia* however, point towards a nutrient-rich environment potentially influenced by upwelling processes, characteristic of Oman's east coast (McLachlan et al., 1998). Alternatively, nutrient enrichment could also be intensified by or result from the decay of algae or proximity to mangrove forests, with nutrient input from sources like crab fecal pellets and mangrove leaves.

Presently, oxygen content in the northern Indian Ocean is reported by the U.S. National Oceanographic Data Centre database to be <0,2 ml

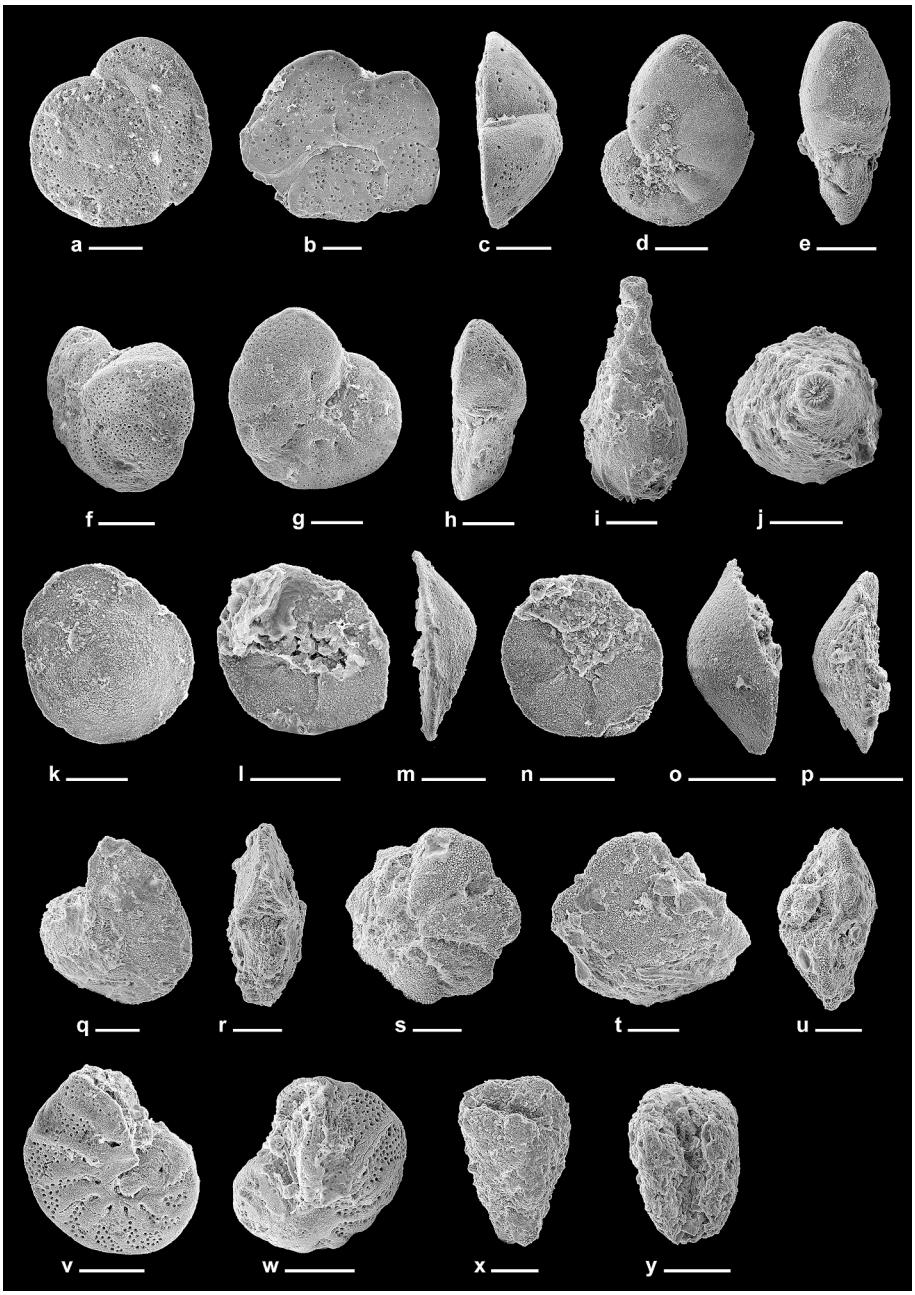


**Fig. 8.** Plate II, scale is 100 μm; a-c) *Lobatula lobatula* different tests of *Lobatula lobatula* are characterized by a different degree of deformation. (a) normal specimen – spiral side (b) moderately deformed specimen – spiral side; d,e) cf. *Pseudononion* sp. 1; f-h) cf. *Lobatula* sp. 1; i,j) *Procerolagena* sp.1; k-m) *Neoconorbina marginata*; n-p) *Neoconorbina multimarginata*; q,r) *Operculina* cf. *ammonoides*; s-u) *Pararotalia* sp. 1; v-w) *Trochulina* sp. 1; x-y) *Valvulina* sp. 1.

$O_2$/l, indicative of a dysoxic, microxic or even anoxic environment (Bernhard and Sen Gupta, 1999). The lack of freshwater input and the presence of oxygen-consuming organisms, including algae, likely exacerbated the reduction in oxygen content. This could have led to oxygen demand exceeding supply, rendering the sediment anoxic.

Lithofacies OR3, is interpreted as a coastal barrier overriding the lagoonal deposit, based on the typical landward dipping foresets overlaying the discordance at the top of OR2 and the shell content indicating marine influence. The clasts observed in OR3 indicate two distinct sediment sources, better rounded components are likely sourced along the southern flanks of the Hajar Mountains and transported to the coast via fluvial and/or alluvial processes, whereas poorly rounded radiolarite fragments stem from local bedrocks. Facies OR4 exhibits cross-bedding and bioturbation within some sandy portions indicating a beach or supratidal backshore setting. Overlying facies OR5 comprises gravel and rounded boulders, representing a fluvial setting and possibly a fanglomerate, formed during a sea-level regression.

In summary, the Ras ar Ru'ays coastal profile reveals a stratigraphy comprising a shallow marine lagoonal stage at the base, overridden by a coastal barrier that stabilised into a beach and, finally, a fanglomerate, indicating a terrestrial environment. This can be interpreted as transgression followed by a regressional phase. The position of the coastal barrier facies at roughly 4 m above pmsl coincides with the paleo shoreline at Sur Lagoon at a same height of 3.5 to 4 m above pmsl. In Sur, a bioerosion notch depicts the former sea level(Falkenroth et al., 2020) and is referred to MIS 5a sea-level highstand within the Last Interglacial by quartz U/Th datings of an associated beachrock deposit which revealed an age of 80 ± 3 ka (Mauz et al., 2015).

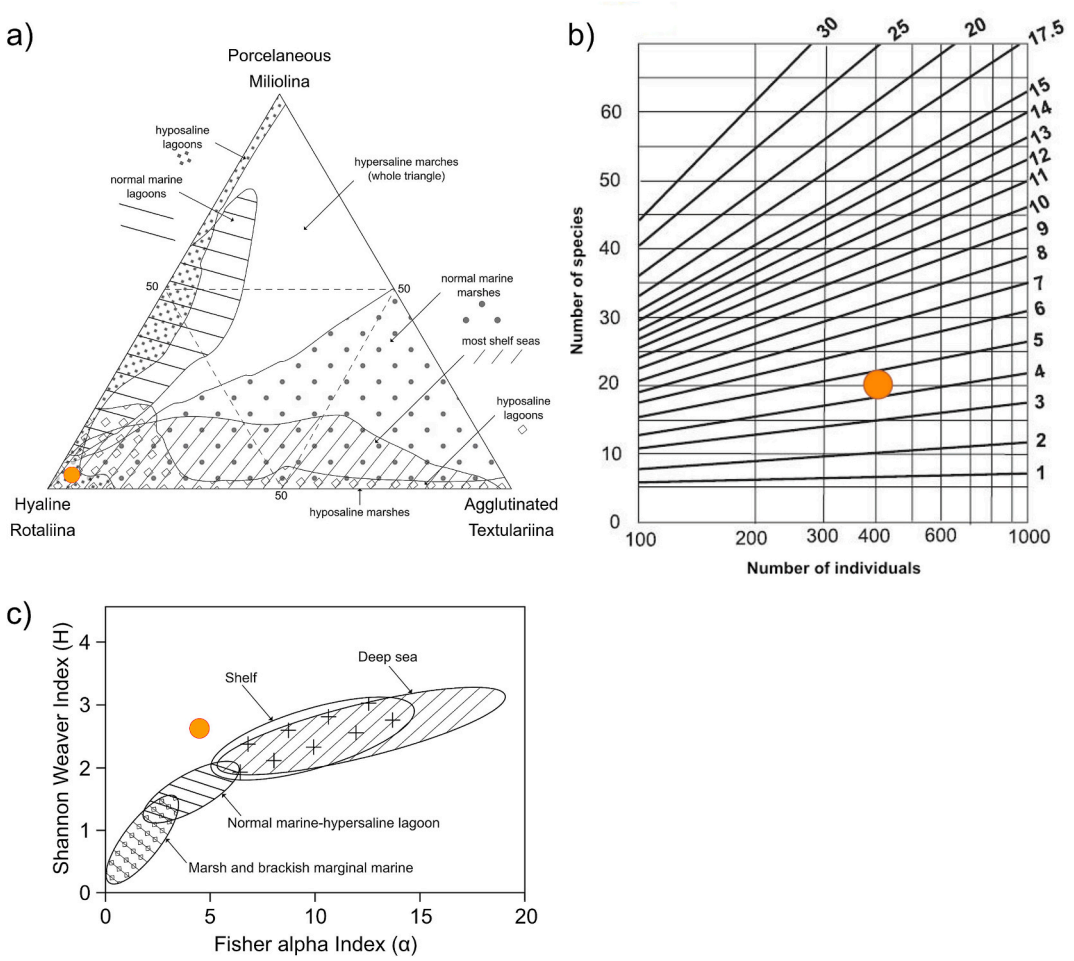


**Fig. 9.** The results of a comprehensive foraminiferal analysis. The sample of OR2, of the coastal profile at Ras ar Ru'ays is marked with an orange dot. a) A ternary diagram of the shell type ratio, differentiating between porcelaneous, hyaline and agglutinated tests, the sample's location in this diagram is not indicative for a specific environment (after Murray, 1991); b) The Fisher-α-index reflects the number of individuals against the number of species, the sample gives a value of 4.5 indicating eutrophic water conditions (after Murray, 1991); c) The Shannon-Weaver-index of the sample amounts to 2.63 and indicates a paleoenvironment of a shelf or lagoon (after Shannon and Weaver, 1949).

### *4.3. Outcrops III a and III b: Ras Madraka I and Ras Madraka II*

In this study two coastal sections with marine facies were identified near Ras Madraka (Ras Madraka I and Ras Madraka II). Both show sandy sediments with some shell debris and molluscs ~4 m above pmsl. While Ras Madraka I is located sheltered inside a small lagoon, Ras Madraka II forms the tip of a headland and is exposed to the rough seaside of the Indian Ocean.

Outcrop Ras Madraka I is located ca. 100 m onshore. Outcropping rocks of the allochthonous Masirah-Ophiolite are unconformably overlain by several layers of consolidated sand, gravel and beachrock. The outcrop is approximately 30 m long and varies in thickness from 1.5 m on the seaward side to 2.5 m on the landward side. One log was measured on the seaward edge. Within this log, three distinct lithofacies (OM1 to OM3) are found overlaying the Ophiolite bedrock (Fig. 10).

Outcrop Ras Madraka II is located just besides the sea, the base of the hill consists of a micritic light grey limestone that belongs to the Miocene Warak Formation. The recent notch is formed within these rocks. This limestone is unconformably overlain by gravelly, sandy deposits. These deposits are attached as patches to the hill (Fig. 11). The limestone is partly covered with cemented rockfall at the base. The measured log at Ras Madraka II displays three distinct lithofacies (OM3 to OM5), one of which is also found at Ras Madraka I (OM3) (Fig. 12).

#### *4.3.1. Sedimentology*

Facies OM1 is a 0.65 m thick, clast-supported conglomerate. Clasts are 0.5 to 6 cm large, subangular and are mostly made up of ophiolite (95 %) and 5 % limestone. The clasts are embedded in a light-beige fine sandy silt-matrix, semi consolidated. Within the outcrop this facies shows few parts with cross-bedding-structures.

Facies OM2is 0.12 m thick and consists of a clast-supported semi-consolidated conglomerate. Clasts are pebble to cobble sized (0.5 to 8 cm diameter), whereas the largest clast fraction is only 5 % of the total. The clasts are rounded ophiolite (ca. 80 %) and shells of bivalves and gastropods (ca. 20 %). Further shell material occurs as debris and is thus impossible to identify. The matrix is a cemented off-white clay-silt.

This 0.1 to 1.1 m thick facies OM3 is a consolidated beige fine to middle sand with planar cross-bedding. Locally, the material contains 1 cm-thick bands of few cm-sized ophiolite clasts in Ras Madraka I. On the seaward side the facies is covered by patches of beachrock, 1 to 2 m in diameter, most likely few centimeter thick. In Ras Madraka I this facies shows one vertical bioturbation structure of ca. 1 cm in diameter. In Ras Madraka II this facies includes various vertical bioturbation structures of ca. 2 cm in diameter.

Facies OM4 is 0.15 to 0.5 m thick and consists of a beige consolidated middle sandy, gravelly coarse sand with rounded grains. The sediment is unsorted and chaotic and contains some incorporated shell debris. In the upper part OM4 includes shell debris and some embedded oyster shells.

Facies OM5 varies from 0.7 and 9.1 m in thickness. The facies

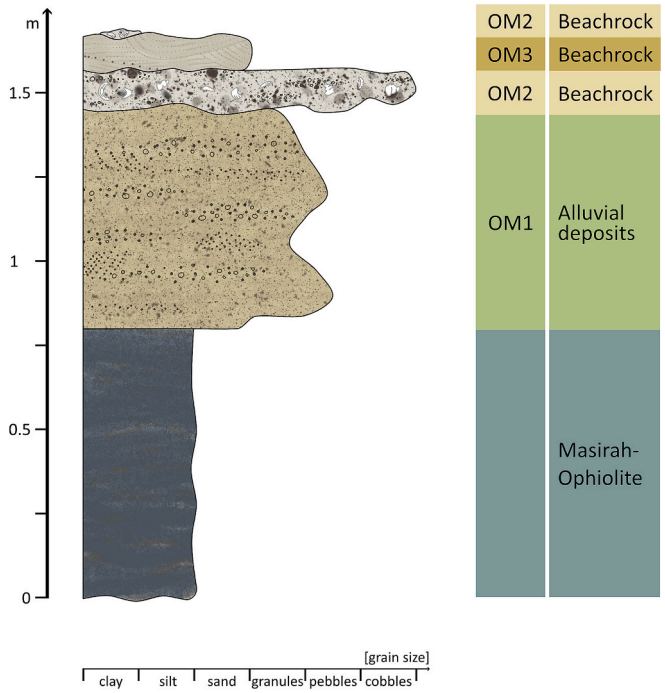


**Fig. 10.** Profile section of the coastal outcrop Ras Madraka I with the Masirah ophiolite at the base, discordantly overlain by alluvial sediments and various beachrock deposits.

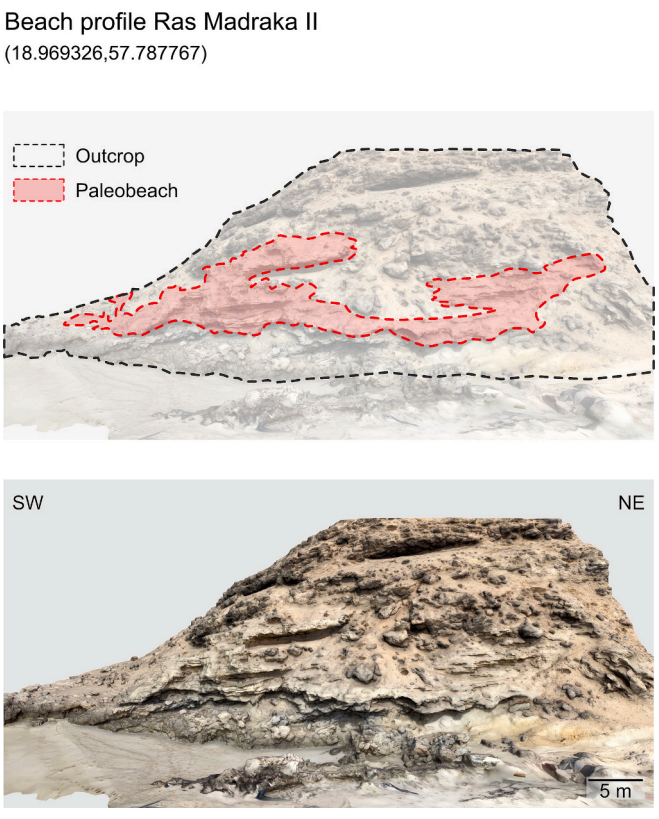


**Fig. 11.** Image taken from a 3D model (Grigowski, 2022) of the coastal outcrop Ras Madraka II; highlighted are the paleobeach findings.

consists of well-sorted, light beige, consolidated fine sandy middle sand with incorporated shell debris and isolated fully preserved mollusc shells. It is a congruent sediment layer showing distinctive features at

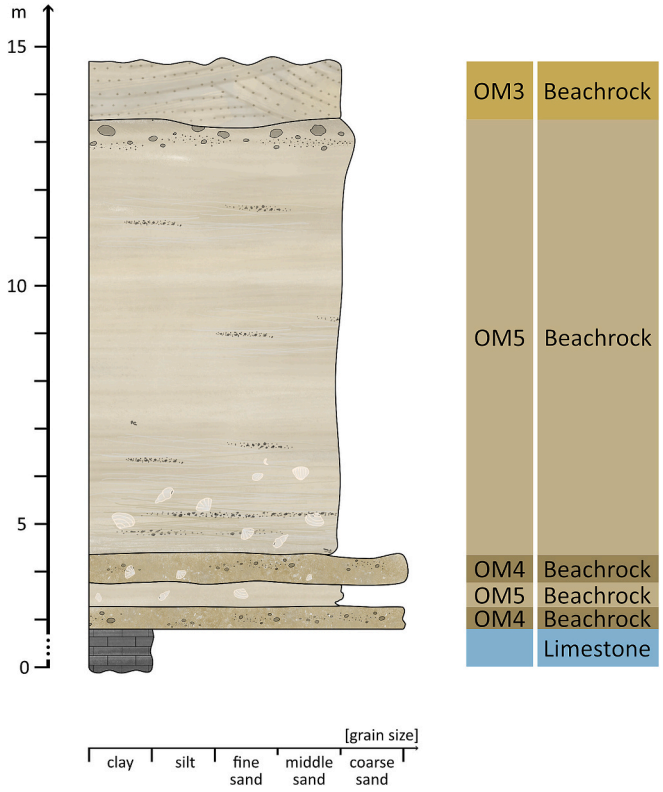


**Fig. 12.** Profile section of the coastal outcrop Ras Madraka II with various beachrock deposits discordantly overlying outcropping limestone.

different heights. At the base of the upper appearance of OM5, within the first 5 cm some bivalve shells are imbricated. The lower 30 cm show 3 lines of gravel and shells, each 2 cm in thickness. Such thin layers can be found occasionally throughout OM5 varying in composition with some consisting of few-cm-sized rock and shell debris and some only of rock clasts, e.g. at 5.9 m. From 7.3 m on the sediment is partly bioturbated. At an elevation of 13.4–13.7 m OM5 shows a high density (ca. 50 %) of incorporated angular, gravel-sized limestone debris that stretches over 30 cm of the profile.

### *4.3.2. Interpretation*

Facies OM1 is a conglomerate formation found exclusively in Ras Madraka I. This facies is characterized by subangular clasts, primarily composed of ophiolithic material, which suggests a very short transportation distance. Such characteristics strongly support the interpretation of a fanglomerate deposition, indicating that these sediments likely originated from local or nearby sources, quickly accumulating in the area.

Facies OM2, found exclusively in Ras Madraka I, is characterized by an abundance of shells and shell debris, which distinctly identify it as a beachrock deposit. Beachrock formations typically form in intertidal or shallow subtidal zones where sediment is cemented by minerals like calcium carbonate, resulting in a solid, rocky structure. The occurrence of conglomerate within this facies indicates that the beach environment was subjected to either significant wave energy or notable fluvial influence.

Facies OM3 is encountered in both Ras Madraka I and II. This facies also represents a beachrock deposit. It exhibits notable features towards its upper layers, such as the presence of mollusc shells and bioturbation structures. These characteristics are indicative of a supratidal backshore environment, suggesting that this region has experienced fluctuations in sea level that allowed for the formation of beachrock structures under varying intertidal conditions.

Facies OM4 and OM5 are exclusive to Ras Madraka II and are both beachrock sediments. However, they represent different depositional environmental settings. OM4 exhibits a somewhat chaotic structure and contains shell debris but also intact shells including oyster shells. OM5, on the other hand, is characterized by finer-grained material, cross-bedding patterns, and an increased occurrence of bioturbation structures. This suggests distinct depositional conditions, with OM4 potentially reflecting more energetic wave conditions, while OM5 represents a quieter, fine-grained beachrock environment.

The presence of these contrasting sedimentary facies within the Ras Madraka region raises several observations:

Despite similar elevations, Ras Madraka I and II showcase differences in sediment characteristics, hinting at varying depositional environments. The coarser sediments in Ras Madraka I suggest the influence of an incoming wadi system, likely transporting larger, coarser materials to this bay. In contrast, Ras Madraka II features finer-grained sediments, suggesting a calm depositional environment within a rocky embayment with a different sediment source.

The presence of angular rock clasts in the upper part of OM5 may be interpreted as hillslope debris. Erosion and changes in coastal morphology might have been influenced by climatic changes, or have been associated with shifts in sea level or wave dynamics.

Both sites, Ras Madraka I and II, exhibit a transgressional conglomerate at their base, indicating a period of sea-level rise followed by highstand and regression. These sedimentary sequences hold valuable information about past sea-level fluctuations and the geological history of this coastal region.

### 4.4. Other outcrops

The following outcrops were not investigated in detail, but provide intriguing evidence of their marine origin, despite their elevation of up to ~4 m above msl.

#### 4.4.1. Outcrop IV: Al Haddah

Close to Al Haddah at the eastern coastline of Oman (Fig. 1 IV), a 4 m high coastal cliff displays several semi consolidated marine and deltaic deposits discordantly overlaying the radiolarian mudstones and pelagic limestones of the Triassic Sal Formation (Peters et al., 2000) (Fig. 13). The profile has already been shortly described by Decker et al. (2021), but has been re-examined in March 2024 and is mentioned here again for completeness.

The base of the profile is made up by coarse sandstones interbedded with granule and pebble layers, that show steep seaward dipping foresets. The components are mostly angular radiolarites and shell fragments. These sandy layers are capped by a 25 cm thick, inversely graded

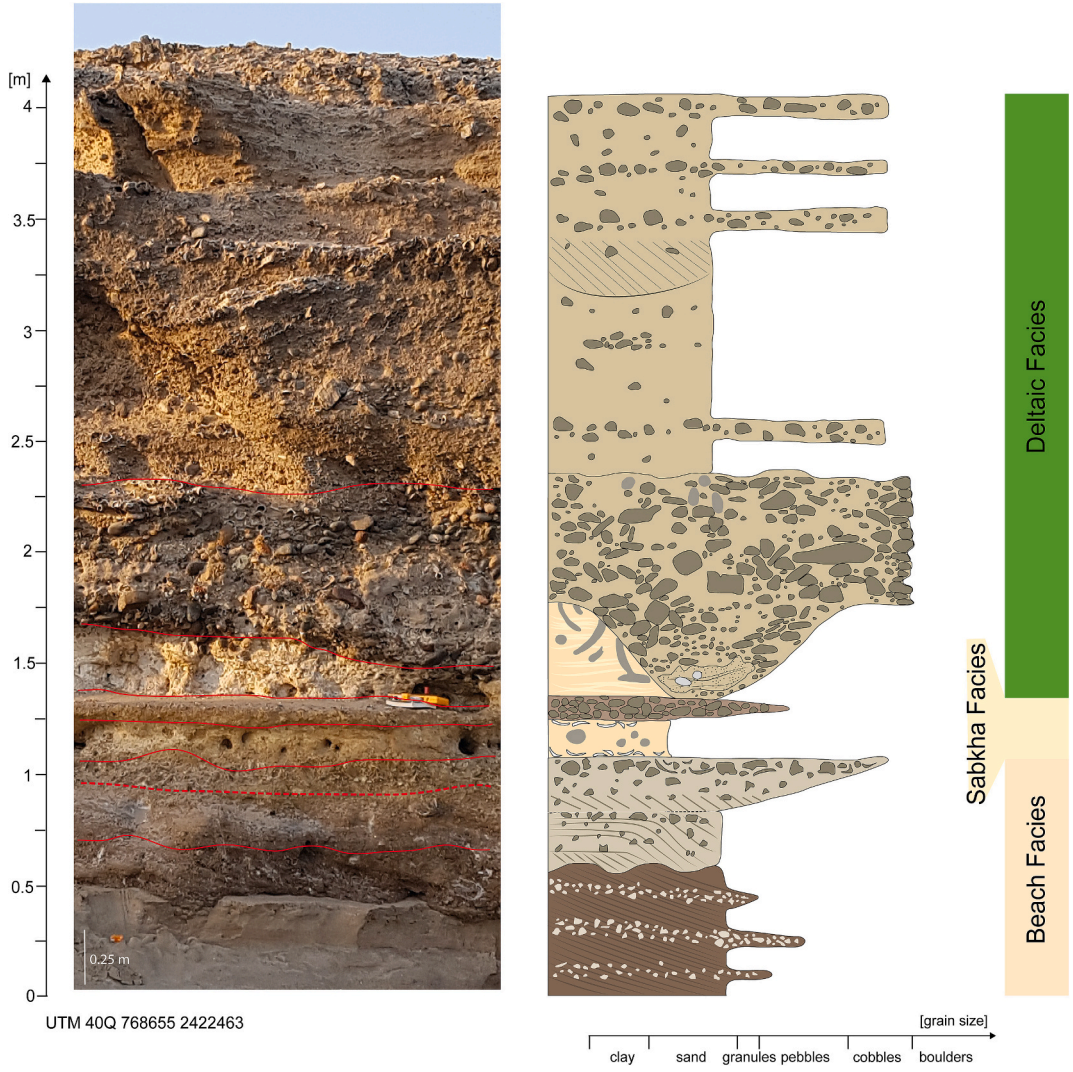


**Fig. 13.** Profile section of the coastal outcrop near Al Haddah, with different layers indicating beach facies deposits at the bottom, followed by sabkha facies deposits and deltaic deposits from ca. 1.5 m onwards towards the top. These deposits include findings of fossil *Crassostrea* oyster shells at various heights.

cobble conglomerate with a chaotic fabric that almost exclusively contains clasts of oyster shell fragments. A sharp but irregular contact is separating the conglomerate from a 0.5 m thick, fine to medium, light yellow sand showing parallel lamination and large burrows as well as a high content of evaporites (salt and gypsum) concentrated in individual laminae. This fine-grained layer is interrupted by another only 0.1 m thick pebble conglomerate with a high shell content. Finally, the upper part of the profile is made up of large cobble to boulder conglomerates that are mostly matrix supported but also display areas of clast supported fabric. The conglomerates show large scale trough cross bedding and channel structures. The clasts in these conglomerates are rounded and more variably than in the layers below containing limestones, ophiolites, radiolarites and large oyster shells of the genus *Crassostrea gryphoides* (Hoffmann et al., 2016).

*Interpretation.* The base of the profile is interpreted as a beach foreshore facies due to the sedimentary structures and clasts content that indicate an exclusively local source. These beach sands are overlain by sabkha deposits characterized by their fine grained sediments and evaporite content. Both the beach facies as well as the sabkha facies are interrupted by high energy events, possibly storms, that eroded an oyster reef and transported high amounts of the shell debris inland. The conglomerates at the top of the profile are interpreted as deltaic facies, based on their structure and clast content that show their connection to a larger feeder system transporting clasts from the southern side of the Al Hajar mountains to the coastline. A similar deltaic facies is also recorded in a nearby 2 m high coastal cliff next to As Sulayb (Decker et al., 2021) where it also contains a substantial quantity of well-preserved *Crassostrea gryphoides* (Hoffmann et al., 2016). The preservation of these shells makes them suitable candidates for dating. However, attempts to date one of the shells from the As Sulayb profile using radiocarbon dating yielded inconclusive results due to the age of the material exceeding the age limit of the method.

#### 4.4.2. Outcrop V: Daymaniyat Island Qafsiyyah

The Daymaniyat Islands are located about 15 km north of the capital city, Muscat, within the Gulf of Oman (Fig. 1 V). The archipelago comprises three distinct islands: two characterized by stable bedrock formations and the third forming a complex of smaller rocky islands interconnected by sand spits. This intricate complex stretches over a distance of approximately 6.5 km. The islands predominantly consist of a micritic to brecciated reddish-beige Miocene limestone that belongs to the Sur Formation of the Fars Group (Wyns et al., 1992) and bears resemblance to the Jafnayn Formation that crops out at Ras al Hadd (Wyns et al., 1992).

On the middle island, Qafsiyyah Island, a notable beachrock outcrop is prominently located along the southern coast, situated at an elevation of approximately 4 m (Fig. 14a). It is located within a sheltered embayment, featuring a thickness of around 2.5 m, which tapers towards its edges, erosive processes created an overhang in the middle of the profile (Fig. 14b). This beachrock formation consists of yellowish-beige, cemented medium to coarse sand, often displaying characteristics such as cross-bedding and bioturbation structures (Fig. 14c). The latter are 1–3 cm in diameter, appear mostly unoriented and show a dark, inner lining (Fig. 14c). They are hollow or filled with coarse sand, differing from the surrounding material (Fig. 14d).

*Interpretation.* The beachrock deposits identified at an elevation of ~4 m on the Daymaniyat Island Qafsiyyah can be associated with a depositional environment within the lower backshore or upper foreshore, reflecting their position within the coastal zone (Falkenroth et al., 2019; Mauz et al., 2015).

#### 4.4.3. Outcrop VI: Ras al Hadd

The village of Ras al Hadd is located on a bedrock that acts as a natural barrier separating a lagoon from the open ocean (Fig. 1 VI). The rock is a micritic beige, partly reddish Late Paleocene to Early Eocene limestone that belongs to the Jafnayn Formation (Wyns et al., 1992). The bedrock is prominently exposed in various locations around the perimeter of the Ras al Hadd lagoon. In this study, particular attention was given to an outcrop situated near the entrance of the Ras al Hadd lagoon. The outcrop is located on private ground. At this site, the bedrock cliff is 6–7 m high and 270 m wide.

The lowermost meter is covered by sessile intertidal organisms, namely oysters and barnacles (Fig. 15a). The barnacles can reach sizes of up to 5 cm in diameter, are found both on the surface and nestled within remnants of oyster shells. Above this overgrown area, an irregular coastal notch has developed (Fig. 15a, white arrow), it shows no signs of




**Fig. 14.** Plate of specific features of the paleobeach on the Daymaniyat Island Qafsiyyah; with a) an overview and the location of the outcrop at the beach, b) a side view of the paleobeach beachrock, c) & d) different bioturbation structures within the beige beachrock, the darker inner lining of the bioturbation channels is clearly visible.

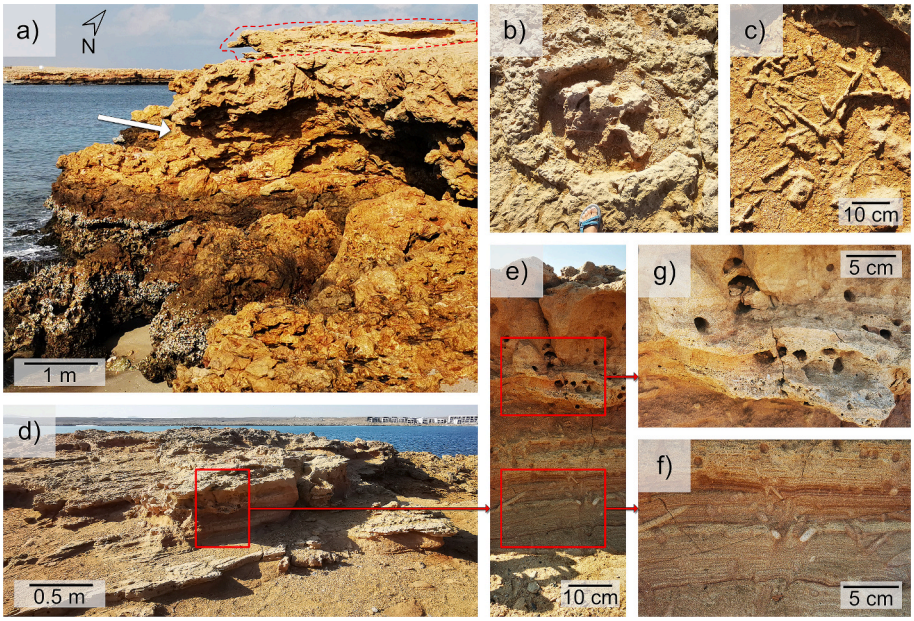


**Fig. 15.** Plate of specific features of the outcrop in Ras al Hadd (on private property, not freely accessible); with a) the recent notch (white arrow) and the location of the beachrock (red dashed line); b) surface: round structure, maybe altered coral; c) surface: mainly horizontal bioturbation structures; d) outcropping beachrock; e) profile of the beachrock; f) magnifying the lower part of the profile with many differently orientated sediment-filled bioturbation structures; g) magnifying the upper part of the profile with bore-hole structures. (For interpretation of the references to colour in this figure legend, the reader is referred to the web version of this article.)

bioerosion, suggesting abrasion as the primary formation process. The apex of this recent notch stands at an elevation of about 3.5 m above msl. The notch has a total height of 1.5 m and a symmetrical u-shaped configuration.

At an elevation of 2 m, the Eocene limestone is overlain by an 8-cm-thick matrix-supported conglomerate. This layer comprises rounded to subangular clasts ranging from 2 to 5 cm in size, featuring various lithologies, primarily limestone and red clay- to siltstone components.

The conglomerate is covered by a sandy beachrock deposit, measuring 1.4 m in thickness (Fig. 15a, red dashed line). The deposit exhibits a normal grading sequence, starting with beige medium to coarse sand at the base, transitioning to a beige to reddish medium sand towards the top. The layers are planar bedded, with a gentle dip of ca. 10° towards SW. The lower beds display distinct crossbedding structures, while the upper layers are characterized by extensive bioturbation (Fig. 15d-g). Tube-like trace fossils are predominantly oriented horizontally, with a few displaying vertical orientations. These trace fossils possess an average diameter of 1 cm, with the largest tube measuring 2 cm in diameter and extending to a length of 30 cm.

*Interpretation.* The coastal cliff at Ras al Hadd features a recent abrasional notch and a beachrock deposit that is ~3–4 m elevated above the

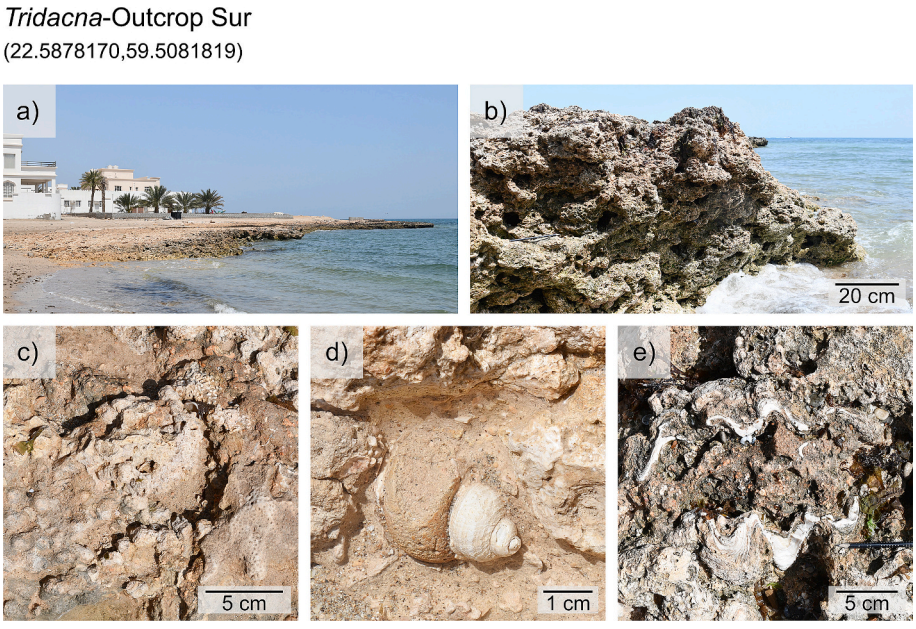


**Fig. 16.** Plate of specific features of the paleoreef in Sur; with a) an overview of the outcrop at the beach, b) picture of the section, c) a close up picture of in situ corals, d) a fossil gastropod shell with partly shell preservation, partly steinkern preservation and e) the fossil shell of an in situ *Tridacna* bivalve.

pmsl. The extensive bioturbation observed within this beachrock layer, along with the absence of marine shells, characterizes it as a beach facies situated within the Lower Backshore or Upper Foreshore zone.

#### 4.4.4. Outcrop VII: Tridacna-outcrop Sur

In the city of Sur, located along the north eastern coastline, an ancient coral reef crops out and spans an area of approximately 900 $m^2$. This paleo reef is elevated to about 0.5 m above mean high tide, which means it is only submerged during spring tide conditions (Fig. 16a & b). It encompasses a diverse array of coral species and other reef-dwelling organisms (Fig. 16c & d). The most striking are shells of the giant clam *Tridacna*, which are found with articulated valves of up to 18 cm length (Fig. 16e). At the top of the fossil reef a wave-cut platform has developed. The upper surface of the platform experiences currently minimal abrasion, whereas the most seaside edge is eroded and undercut by waves.

*Interpretation.* The presence of *Tridacna* shells serves as an indicator of the original water depth, which ranged from 0 up to 20 m below sea level at its maximum (Hardy and Hardy, 1969). Today, the giant bivalve *Tridacna* inhabits shallow coral reef areas in the Indo-Pacific region, where it can be found either resting unattached on the seafloor or firmly anchored within coral reefs, using robust byssus threads (Hardy and Hardy, 1969). The latter situation aligns with our discoveries in Sur, where it is presumed that the ancient fossil reef formed within the Lower Shoreface Zone.

## 5. Discussion

There are two main points that need to be discussed: the question of a potential Mid Holocene sea-level highstand in the area and field evidence for older, most likely Late Pleistocene (MIS 5) coastal deposits.

In a global context, Mid Holocene sea-level highstands are reported (Mauz et al., 2022; Lambeck et al., 2002; Blum et al., 2001), however the spatial timing and amplitude of rsl-changes vary significantly worldwide (Li et al., 2023 and references therein). Khan et al. (2015) give an overview on global Holocene rsl-variations for near-field, intermediate-field and far-field regions. Though they do not provide site-specific data, neither for India nor the Arabian shoreline, comparable far-field regions like south-east Asia, southern China and South America provide evidence for a Mid-Holocene sea-level highstand. The timing ranges from 8 to 4 ka BP and the height from <1 to 6 m (Khan et al., 2015). Additionally, Holocene sea-level highstands are reported worldwide, e.g. from Australia (Lambeck et al., 2002), India (Bhatt and Bhonde, 2006; Nakada and Lambeck, 1987) and America (Blum et al., 2001). In Yemen, directly southwest of Oman, paleo notches and fossils like corals, indicate a Mid Holocene sea-level highstand which exceeded heights of approximately 0.5 to 1 m above pmsl; U-series chronology on in situ found *Porites* sp. and *Acropora* sp. corals dated these deposits to 5 to 5.4 ka (Al-Mikhlafi et al., 2021). A sea-level highstand of 1.6 ± 0.4 m is reported by Mauz et al. (2022) for the Arabian Gulf in the period 6.7–6.0 ka. A potential South Pacific eustatic Late Holocene highstand of 0.9 m above pmsl between 6 and 1.2 ka BP was postulated by Pirazzoli and Montaggioni (1986).

To our knowledge, no prior mapping focussing on deposits that indicate a Holocene sea-level highstand has been undertaken along the coastline of Oman. Nevertheless, some authors, such as Lézine et al. (2002) and Berger et al. (2020) have reported isolated, single findings that were interpreted as indicative of a Holocene sea-level highstand of 1–2 m (Lézine et al., 2002) or 9 m (Berger et al., 2020). Late Holocene marine deposits, approximately 1000 years old, at elevations of up to 15 m above pmsl in the Tiwi-area have been distinctly characterized as extreme wave deposits (Hoffmann et al., 2020b). As such, these deposits near Tiwi are not suitable for reconstructing Holocene rsl. Decker et al. (2021) reported on Holocene lagoonal deposits along the north eastern coast around Ras ar Ru'ays. These 6 ka old paleo mangrove environments are at an elevation above pmsl similar to recent mangrove habitats nearby, thereby excluding a Holocene sea-level highstand during the Mid-Holocene. The marine deposits described here support this, as there is currently no evidence for Holocene shorelines higher than that of the present level. More plausible is that the marine deposits described are associated with a Late Pleistocene sea-level highstand during MIS 5, which has been proven for the area around Sur (Falkenroth et al., 2020). The area is regarded as tectonically stable, an important requirement to disentangle the contributions of various processes (Lambeck et al., 2014, 2002).

We postulate that all coastal deposits described here are of Late Pleistocene age as there is no evidence for a Holocene sea-level highstand in the study area. Several factors support this hypothesis: (a) The coastal profile at Tiwi exhibits an abrasion platform as the uppermost facies, a marine terrace (MIS 5a (Hoffmann et al., 2020a)) belonging to the terraces of the Fins area. Consequently, all underlying layers are significantly older than 82 ka. The echinoderm shells of *Echinometra mathaei* suggest a maximum age of Late Pleistocene, as this is the oldest finding of that species in the eastern Indian Ocean area (Philippe, 1998). (b) In Sur, the paleo notch, along with the associated paleo beach, is located approximately 3.5 m above pmsl. Quartz grains of the paleo beachrock were dated using OSL, leading to an age of 80 ka ± 3 ka and their attribution to MIS 5e (Eemian) (Mauz et al., 2015). The *Tridacna* exposure at the beach lies just above the pmsl. *Tridacna* inhabits water depths ranging from 0 to 20 m (Hardy and Hardy, 1969). The relative elevation difference between the fossil coral reef with in-situ *Tridacnae* and the paleo notch with paleo beach permits the correlation of these exposures. Thus, the *Tridacna* exposure can be assigned to the Late Pleistocene sea-level highstand during MIS 5e. (c) Radiocarbon dating of the *Crassostrea* mussel shell from As Sulayb exceeds the dating method's age limit and therefore provides a minimum age of 45 ka. (d) The deltaic deposits in the upper outcrop areas in Al Haddah and As Sulayb and in the middle part of the outcrop in Ras ar Ru'ays can be correlated with similar facies in a nearby outcrop, studied by Berger et al. (2019). This conglomerate was OSL-dated to 437,983 ± 76,332 BCE and indicates a Pleistocene fluvial-deltaic formation. (e) This coastal section in north eastern Oman is considered tectonically stable, at least within the last 6000 years (Decker et al., 2021). Thus, the coastal profile at Ras ar Ru'ays indicates sea-level oscillations or uplift that must be considerably older than 6000 years.

Evidence of Last Interglacial sea-level highstands are reported worldwide (e.g. Rovere et al., 2023; Boyden et al., 2021; Pedoja et al., 2011; Banerjee, 2000). The results presented here contribute to the ongoing effort to identify new outcrops, develop approaches, investigate past sea-level changes and finally model sea-level scenarios (Chauveau et al., 2024b; Boyden et al., 2023; de Gelder et al., 2022). Such research aligns with initiatives such as the PALSEA project (PALeo constraints on SEA level rise) (Rovere and Dutton, 2021). Most notably amongst the project's outputs, is the recently launched WALIS Explorer database (World Atlas of Last Interglacial Shorelines), introduced by Rovere et al. (2022).

Future research in this area can use the findings from this study as a starting point. Most valuable would be a systematic dating of the sequences described. However, material suitable for dating is limited in this area due to depositional and climate conditions. In particular, recrystallization of primarily aragonitic corals has rendered Uranium-Thorium dating impractical (oral communications, Lars Reuning), as observed at the Tiwi cliff (refer to Section 4.1.), also Kellerhals (1998) encountered similar difficulties with dating in his study area south east of Tiwi. Radiocarbon dating of shells has proven unreliable due to the age of the material exceeding the dating method's limits which lie in the range of 40–45 ka BP (Törnqvist et al., 2015). This same issue was encountered by Moraetis et al. (2018) and Mattern et al. (2018) when endeavouring to establish an age model for the marine terraces near Fins. The dating and correlation of the marine terraces at Fins were

resolved by Hoffmann et al. (2020a), based on an age model using cosmogenic nuclides $^{10}$Be and $^{36}$Cl. The measurement of the nuclide concentrations reflects the surface exposure, the timespan since when the material, rock or coral, has been exposed to the sun (Ivy-Ochs and Kober, 2008). However, this dating method results in large uncertainties which will hamper its potential in rsl studies. OSL dating poses certain complexities due to the prevalent nature of carbonate deposits, which are the primary source materials for clastic sediments. An exception can be found along the coastline to the south of Ras al Hadd, where igneous source rocks supply quartz and feldspar that could potentially be suitable for OSL dating (Berger et al., 2020). Therefore, this area presents a promising prospect for future dating endeavours.

## 6. Conclusions

This study is a comprehensive coastal mapping effort covering the shoreline of northeastern Oman, ranging from the area around Muscat in the north to Ras Madraka in the south. The sedimentary deposits documented here, encompassing shallow marine to beach facies, represent coastal formations that are currently situated above mean sea level. These accumulations deviate from their expected locations under current sea-level conditions, suggesting influences such as eustatic sea-level oscillations, coastal uplift, or a combination of both.

In regions with tectonically stable coasts, particularly along the east coast, these deposits likely reflect eustatic sea-level oscillations. Notably, this pattern is observed in the outcrops around Sur, Ras al Hadd, Ras ar Ru'ays, and Ras Madraka. These outcrops provide evidence of an ancient sea-level highstand, approximately 3–4 m above present mean sea level. Dating these deposits proved difficult. Evidence for a Holocene sea-level highstand was not identified. We tentatively assign a Late Pleistocene age to the deposits and argue that they likely formed during MIS 5.

These descriptions serve as an initial orientation and localisation guide for these outcrops, highlighting the potential for further in-depth investigations. In subsequent projects or investigations, all outcrops should be surveyed using Differential Global Positioning System. Additionally, dating of sediments at these sites would provide valuable insights and allow to define sea-level index points. Hereby, these outcrops will become few of the many glimpses into past sea levels that are needed to obtain a verified view into sea-level history worldwide. Only through this we will understand processes and help to estimate future sea-level oscillations.

## Funding

VD is grateful for a scholarship provided by the Studienstiftung des deutschen Volkes. Furthermore, this paper stands as a contribution to the IGCP projects 639 and 725.

## CRediT authorship contribution statement

**V. Decker:** Writing – review & editing, Writing – original draft, Visualization, Conceptualization. **M. Falkenroth:** Writing – review & editing, Writing – original draft, Visualization. **G. Hoffmann:** Writing – review & editing, Writing – original draft, Conceptualization.

## Declaration of Generative AI and AI-assisted technologies in the writing process

Statement: During the preparation of this work the authors used ChatGPT in order to improve the language and readability. After using this tool/service, the authors reviewed and edited the content as needed and takes full responsibility for the content of the publication.

## Declaration of competing interest

The authors declare that they have no known competing financial interests or personal relationships that could have appeared to influence the work reported in this paper.

## Data availability

All data used for this work have been collected and processed by ourselves. Additional data related to this article can be found at (https://data.mendeley.com/datasets/6yx52x7cvv/1), an open source online data repository hosted at Mendeley Data.

## Acknowledgements

Prof. Dr. Martin Langer (University of Bonn) is thanked for his invaluable assistance in conducting foraminiferal analyses, which includes species identification and interpretation. We are also grateful for his provision of technical support and access to essential equipment. Our acknowledgment extends to Olaf Dülfer (University of Bonn) for his indispensable contributions in the laboratory.

Special thanks are due to Martha Berens (University of Bonn), whose support in the realm of REM pictures and visual preparation has been crucial to this paper. Additionally, we express our gratitude to Edouard Grigowski (University of Bonn) who skillfully processed the 3D model for Ras Madraka II.

Our heartfelt appreciation goes to the Golden Highlands team in Oman for their exceptional logistic support during our field campaigns. We extend our thanks to Kim Hußmann for her tireless efforts and invaluable assistance in managing the fieldwork.

Clare Bamford is gratefully thanked for the English review.

We thank three anonymous reviewers for their time and effort and their critical comments that helped to improve the quality and readability of the manuscript significantly.

## References

Al-Farraj, A., 2005. An evolutionary model for sabkha development on the north coast of the UAE. J. Arid Environ. 63 (4), 740–755.

Al-Mikhlafi, A.S., Hibbert, F.D., Edwards, L.R., Cheng, H., 2021. Holocene relative sea-level changes and coastal evolution along the coastlines of Kamaran Island and As-Salif Peninsula, Yemen, southern Red Sea. Quat. Sci. Rev. 252, 106719.

Banerjee, P.K., 2000. Holocene and late Pleistocene relative sea level fluctuations along the east coast of India. Mar. Geol. 167 (3–4), 243–260.

Bange, H.W., Bathmann, U., Behrens, J., Dahlke, F., Ebinghaus, R., Ekau, W., Emeis, K.-C., et al., 2017. Coasts – A Vital Habitat Under Pressure. World Ocean Review: Living with the Oceans 5. Maribus, Hamburg, Germany.

Barlow, N.L., McClymont, E.L., Whitehouse, P.L., Stokes, C.R., Jamieson, S.S., Woodroffe, S.A., Sanchez-Montes, M.L., 2018. Lack of evidence for a substantial sea-level fluctuation within the last Interglacial. Nat. Geosci. 11 (9), 627–634.

Béchennec, F., Le Métour, J., Platel, J.P., Roger, J., 1993. Geological Map of the Sultanate of Oman. Scale 1: 1.000. 000, with Explanatory Notes. Directorate General of Minerals, Oman Ministry of Petroleum and Minerals.

Berger, J.F., Charpentier, V., Crassard, R., Martin, C., Davtian, G., López-Sáez, J.A., 2013. The dynamics of mangrove ecosystems, changes in sea level and the strategies of Neolithic settlements along the coast of Oman (6000–3000 cal. BC). J. Archaeol. Sci. 40 (7), 3087–3104.

Berger, J.F., Guilbert-Berger, R., Marrast, A., Munoz, O., Guy, H., Barra, A., Béarez, P., 2020. First contribution of the excavation and chronostratigraphic study of the Ruways 1 Neolithic shell midden (Oman) in terms of Neolithisation, palaeoeconomy, social-environmental interactions and site formation processes. Arab. Archaeol. Epigr. 31 (1), 32–49.

Bernhard, J.M., Sen Gupta, B.K., 1999. Foraminifera of oxygen-depleted environments. In: Sen Gupta, B.K. (Ed.), Modern Foraminifera. Kluwer Publishers, Great Britain, pp. 201–216.

Bhatt, N., Bhonde, U., 2006. Geomorphic expression of late Quaternary Sea level changes along the southern Saurashtra coast, western India. J. Earth Syst. Sci. 115, 395–402.

Blum, M.D., Misner, T.J., Collins, E.S., Scott, D.B., Morton, R.A., Aslan, A., 2001. Middle Holocene Sea-level rise and highstand at +2 m, Central Texas coast. J. Sediment. Res. 71 (4), 581–588.

Bosworth, W., Taviani, M., 1996. Late Quaternary reorientation of stress field and extension direction in the southern Gulf of Suez, Egypt: evidence from uplifted coral terraces, mesoscopic fault arrays, and borehole breakouts. Tectonics 15 (4), 791–802.

Boyden, P., Weil-Accardo, J., Deschamps, P., Oppo, D., Rovere, A., 2021. Last interglacial sea-level proxies in East Africa and the Western Indian Ocean. Earth Syst. Sci. Data 13, 1633–1651. https://doi.org/10.5194/essd-13-1633-2021.

Boyden, P., Stocchi, P., Rovere, A., 2023. Refining patterns of melt with forward stratigraphic models of stable Pleistocene coastlines. Earth Surf. Dyn. 11 (5), 917–931. https://doi.org/10.5194/esurf-11-917-2023, 2023.

Brasier, M.D., 1980. Microfossils. Allen & Unwin, London.

Burns, S.J., Fleitmann, D., Matter, A., Neff, U., Mangini, A., 2001. Speleothem evidence from Oman for continental pluvial events during interglacial periods. Geology 29 (7), 623–626.

Cerrone, C., Vacchi, M., Fontana, A., Rovere, A., 2021a. Last Interglacial Sea-level proxies in the western Mediterranean. Earth Syst. Sci. Data 13, 4485–4527. https://doi.org/10.5194/essd-13-4485-2021.

Cerrone, C., Ascione, A., Robustelli, G., Tuccimei, P., Soligo, M., Balassone, G., Mormone, A., 2021b. Late Quaternary uplift and sea level fluctuations along the Tyrrhenian margin of Basilicata-northern Calabria (southern Italy): New constraints from raised paleoshorelines. Geomorphology 395, 107978.

Chauveau, D., Authemayou, C., Pedoja, K., Molliex, S., Husson, L., Scholz, D., Aster Team, 2021. On the generation and degradation of emerged coral reef terrace sequences: first cosmogenic 36Cl analysis at Cape Laundi, Sumba Island (Indonesia). Quat. Sci. Rev. 269, 107144. https://doi.org/10.1016/j.quascirev.2021.107144.

Chauveau, D., Pastier, A.M., de Gelder, G., Husson, L., Authemayou, C., Pedoja, K., Cahyarini, S.Y., 2024a. Unravelling the morphogenesis of coastal terraces at Cape Laundi (Sumba Island, Indonesia): Insights from numerical models. Earth Surf. Process. Landf. 49 (2), 549–566. https://doi.org/10.1002/esp.5720.

Chauveau, D., Georgiou, N., Cerrone, C., Dean, S., Rovere, A., 2024b. Sea-level oscillations within the last Interglacial: insights from coral reef stratigraphic forward modelling. Quat. Sci. Rev. 336, 108759. https://doi.org/10.1016/j.quascirev.2024.108759.

Church, J.A., Gregory, J.M., Huybrechts, P., Kuhn, M., Lambeck, K., Nhuan, M.T., Woodworth, P.L., 2001. Changes in sea level. In: Houghton, J.T., Ding, Y., Griggs, D. J., Noguer, M., Van der Linden, P.J., Dai, X., Maskell, K., Johnson, C.A. (Eds.), Climate Change 2001: The Scientific Basis: Contribution of Working Group I to the Third Assessment Report of the Intergovernmental Panel, pp. 639–694.

de Gelder, G., Husson, L., Pastier, A.M., Fernández-Blanco, D., Pico, T., Chauveau, D., Pedoja, K., 2022. High interstadial sea levels over the past 420 ka from the Huon Peninsula, Papua New Guinea. Commun. Earth Environ. 3 (1), 256.

De Giosa, F., Scardino, G., Vacchi, M., Piscitelli, A., Milella, M., Ciccolella, A., Mastronuzzi, G., 2019. Geomorphological signature of late Pleistocene Sea level oscillations in Torre Guaceto marine protected area (Adriatic Sea, SE Italy). Water 11 (11), 2409.

De Santis, V., Scardino, G., Scicchitano, G., Meschis, M., Montagna, P., Pons-Branchu, E., Ortiz, J.E., Sánchez-Palencia, Y., Caldara, M., 2023. Middle-late Pleistocene chronology of palaeoshorelines and uplift history in the low-rising to stable Apulian foreland: Overprinting and reoccupation. Geomorphology 421, 108530.

Decker, V., Falkenroth, M., Lindauer, S., Landgraf, J., Al-Lawati, Z., Al-Rahbi, H., Franz, S.O., Hoffmann, G., 2021. Collapse of Holocene mangrove ecosystems along the coastline of Oman. Quat. Res. 100, 52–76.

Decker, V., Gee, C.T., Schucht, P.J., Lindauer, S., Hoffmann, G., 2022. Life on the edge: a powerful tsunami overwhelmed indian ocean mangroves one millennium ago. Forests 13 (6), 922.

Decker, V., Falkenroth, M., Hoffmann, G., 2024. Dataset for sedimentological evidence of Pleistocene shorelines in Oman. Mendeley Data V1. https://doi.org/10.17632/6yx52x7cvv.1.

Deiana, G., Antonioli, F., Moretti, L., Orrù, P.E., Randazzo, G., Lo Presti, V., 2021. MIS 5.5 highstand and future sea level flooding at 2100 and 2300 in tectonically stable areas of Central Mediterranean Sea: Sardinia and the Pontina Plain (Southern Latium), Italy. Water 13 (18), 2597. https://doi.org/10.3390/w13182597.

Dullo, W.C., 1990. Facies, fossil record, and age of Pleistocene reefs from the Red Sea (Saudi Arabia). Facies 22 (1), 1–45.

Dullo, W.C., 2005. Coral growth and reef growth: a brief review. Facies 51 (1), 33–48. https://doi.org/10.1007/s10347-005-0060-y.

Dumitru, O.A., Dyer, B., Austermann, J., Sandstrom, M.R., Goldstein, S.L., D'Andrea, W. J., et al., 2023. Last interglacial global mean sea level from high-precision U-series ages of Bahamian fossil coral reefs. Quat. Sci. Rev. 318, 108287. https://doi.org/10.1016/j.quascirev.2023.108287.

Dutton, A., Lambeck, K., 2012. Ice volume and sea level during the last interglacial. Science 337 (6091), 216–219.

Dyer, B., Austermann, J., D'Andrea, W.J., Creel, R.C., Sandstrom, M.R., Cashman, M., et al., 2021. Sea-level trends across the Bahamas constrain peak last interglacial ice melt. Proc. Natl. Acad. Sci. USA 118 (33), e2026839118. https://doi.org/10.1073/pnas.2026839118.

Engel, M., Matter, A., Parker, A.G., Parton, A., Petraglia, M.D., Preston, G.W., Preusser, F., 2017. Lakes or wetlands? A comment on 'The middle Holocene climatic records from Arabia: Reassessing lacustrine environments, shift of ITCZ in Arabian Sea, and impacts of the southwest Indian and African monsoons' by Enzel et al. Glob. Planet. Chang. 148, 258–267.

Enzel, Y., Quade, J., Kushnir, Y., 2017. Response to Engel et al.(in press): Lakes or wetlands? A comment on "the middle Holocene climatic records from Arabia: reassessing lacustrine environments, shift of ITCZ in Arabian Sea, and impacts of the southwest Indian and African monsoons" by Enzel et al. 2015. Glob. Planet. Chang. 100 (148), 268–271.

Enzel, Y., Kushnir, Y., Quade, J., 2015. The middle Holocene climatic records from Arabia: Reassessing lacustrine environments, shift of ITCZ in Arabian Sea, and impacts of the southwest Indian and African monsoons. Glob. Planet. Chang. 129, 69–91.

Erlandson, J.M., 2017. Coastlines, Marine Ecology, and Maritime Dispersals in Human History. Human Dispersal and Species Movement: From Prehistory to Present. Cambridge University Press, Cambridge, pp. 147–163.

Ermertz, A., Kázmér, M., Adolphs, S., Falkenroth, M., Hoffmann, G., 2019. Geoarchaeological evidence for the decline of the medieval city of Qalhat, Oman. Open Quat. 5 (8), 1–14.

Falkenroth, M., Schneider, B., Hoffmann, G., 2019. Beachrock as sea-level indicator–a case study at the coastline of Oman (Indian Ocean). Quat. Sci. Rev. 206, 81–98.

Falkenroth, M., Adolphs, S., Cahnbley, M., Bagci, H., Kázmér, M., Mechernich, S., Hoffmann, G., 2020. Biological indicators reveal small-scale sea-level variability during MIS 5e (Sur, Sultanate of Oman). Open Quat. 6 (1), 1–20. https://doi.org/10.5334/oq.72.

Grigowski, E., 2022. 3D Model Ras Madraka 2023. https://sketchfab.com/3d-models/ras-madraka-dcf50a64861747188ae7b15556822548 (Last access 10th December 2023).

Haigh, I.D., Wahl, T., Rohling, E.J., Price, R.M., Pattiaratchi, C.B., Calafat, F.M., Dangendorf, S., 2014. Timescales for detecting a significant acceleration in sea level rise. Nat. Commun. 5 (1), 3635. https://doi.org/10.1038/ncomms4635.

Hardy, J.T., Hardy, S.A., 1969. Ecology of tridacna in Palau. Pac. Sci. 23, 467–472.

Harrison, J.V., 1941. Coastal makran. Geogr. J. 97 (1), 1–15.

Heidarzadeh, M., Satake, K., 2017. A combined earthquake–landslide source model for the tsunami from the 27 November 1945 M w 8.1 Makran Earthquake. Bull. Seismol. Soc. Am. 107 (2), 1033–1040.

Hibbert, F.D., Rohling, E.J., Dutton, A., Williams, F.H., Chutcharavan, P.M., Zhao, C., Tamisiea, M.E., 2016. Coral indicators of past sea-level change: a global repository of U-series dated benchmarks. Quat. Sci. Rev. 145, 1–56.

Hijma, M.P., Engelhart, S.E., Törnqvist, T.E., Horton, B.P., Hu, P., Hill, D.F., 2015. A protocol for a geological sea-level database. Handbook Sea-level Res. 536–553.

Hoffmann, G., Rupprechter, M., Al Balushi, N., Grützner, C., Reicherter, K., 2013. The impact of the 1945 Makran tsunami along the coastlines of the Arabian Sea (Northern Indian Ocean) – A review. Z. Geomorphol. 57 (4), 257–277.

Hoffmann, G., Meschede, M., Zacke, A., Al Kindi, M., 2016. Field Guide to the Geology of Northeastern Oman.

Hoffmann, G., Schneider, B., Mechernich, S., Falkenroth, M., Dunai, T., Preusser, F., 2020a. Quaternary uplift along a passive continental margin (Oman, Indian Ocean). Geomorphology 350, 106870.

Hoffmann, G., Grützner, C., Schneider, B., Preusser, F., Reicherter, K., 2020b. Large Holocene tsunamis in the northern Arabian Sea. Mar. Geol. 419, 106068.

Imbrie, J., Imbrie, J.Z., 1980. Modeling the climatic response to orbital variations. Science 207 (4434), 943–953.

Imbrie, J., Hays, J., Martinson, D., McIntyre, A., Mix, A., Morley, J.J., Pisias, N., Prell, W., Shackleton, N., Berger, A., Kukla, G., Saltzman, B., 1984. In: Milankovitch, Climate, Berger, A., et al. (Eds.), The Orbital Theory of Pleistocene Climate: Support from a Revised Chronology of the Marine d18O Record. Kluwer Academic Publishers (Nato ASI Ser. C), Dordrecht, pp. 269–305.

IPCC, 2023. Sections. In: Core writing Team, Lee, H., Romero, J. (Eds.), Climate Change 2023: Synthesis Report. Contribution of Working groups I, II and III to the Sixth. Assessment Report of the Intergovernmental Panel on climate Change. IPCC, Geneva, Switzerland, pp. 35–115. https://doi.org/10.59327/IPCC/AR6-9789291691647.

Ivy-Ochs, S., Kober, F., 2008. Surface exposure dating with cosmogenic nuclides. E&G Quat. Sci. J. 57 (1/2), 179–209.

Kellerhals, P., 1998. Ice Age Related Erosional and Depositional Processes. Examples from the Late Proterozoic and Quaternary, Sultanate of Oman.

Khan, N.S., Ashe, E., Shaw, T.A., Vacchi, M., Walker, J., Peltier, W.R., Kopp, R.E., Horton, B.P., 2015. Holocene relative sea-level changes from near-, intermediate-, and far-field locations. Curr. Clim. Chang. Rep. 1, 247–262.

Kukowski, N., Schillhorn, T., Flueh, E.R., Huhn, K., 2000. Newly identified strike-slip plate boundary in the northeastern Arabian Sea. Geology 28 (4), 355–358.

Kwarteng, A.Y., Dorvlo, A.S., Vijaya Kumar, G.T., 2009. Analysis of a 27-year rainfall data (1977–2003) in the Sultanate of Oman. Int. J. Climatol. 29, 605–617.

Lajoie, K.R., 1986. Coastal tectonics. Active Tecton. 95–124.

Lambeck, K., Esat, T.M., Potter, E.K., 2002. Links between climate and sea levels for the past three million years. Nature 419 (6903), 199–206.

Lambeck, K., Rouby, H., Purcell, A., Sun, Y., Sambridge, M., 2014. Sea level and global ice volumes from the last Glacial Maximum to the Holocene. Proc. Natl. Acad. Sci. 111 (43), 15296–15303.

Lézine, A.M., Saliège, J.F., Mathieu, R., Tagliatela, T.L., Mery, S., Charpentier, V., Cleuziou, S., 2002. Mangroves of Oman during the late Holocene; climatic implications and impact on human settlements. Veg. Hist. Archaeobotany 11, 221–232.

Lézine, A.M., Ivory, S.J., Braconnot, P., Marti, O., 2017. Timing of the southward retreat of the ITCZ at the end of the Holocene Humid Period in Southern Arabia: Data-model comparison. Quat. Sci. Rev. 164, 68–76.

Li, T., Chua, S., Tan, F., Khan, N.S., Shaw, T.A., Majewski, J., Horton, B.P., 2023. Glacial Isostatic Adjustment modelling of the mid-Holocene Sea-level highstand of Singapore and Southeast Asia. Quat. Sci. Rev. 319, 108332.

Mattern, F., Moraetis, D., Abbasi, I., Al Shukaili, B., Scharf, A., Claereboudt, M., Looker, E., Al Haddabi, N., Pracejus, B., 2018. Coastal dynamics of uplifted and emerged late Pleistocene near-shore coral patch reefs at fins (eastern coastal Oman, Gulf of Oman). J. Afr. Earth Sci. 138, 192–200.

Mauz, B., Vacchi, M., Green, A., Hoffmann, G., Cooper, A., 2015. Beachrock: a tool for reconstructing relative sea level in the far-field. Mar. Geol. 362, 1–16.

Mauz, B., Shen, Z., Alsuwaidi, M., Melini, D., Spada, G., Purkis, S.J., 2022. The mid-Holocene sea-level change in the Arabian Gulf. Holocene 32 (11), 1173–1183. https://doi.org/10.1177/09596836221114291.

McGranahan, G., Balk, D., Anderson, B., 2007. The rising tide: assessing the risks of climate change and human settlements in low elevation coastal zones. Environ. Urban. 19 (1), 17–37. https://doi.org/10.1177/0956247807076960.
McLachlan, A., Fisher, M., Al-Habsi, H.N., Al-Shukairi, S.S., Al-Habsi, A.M., 1998. Ecology of sandy beaches in Oman. J. Coast. Conserv. 4, 181–190.
Milankovitch, M.M., 1941. Canon of insolation and the iceage problem. Koniglich Serbische Akademice Beograd Special Publ. 132.
Milne, G.A., 2009. Using models to inform the field community: Far-field Sea level data applications. AGES News 17 (2), 56–57.
Milne, G.A., Mitrovica, J.X., 2008. Searching for eustasy in deglacial sea-level histories. Quat. Sci. Rev. 27 (25–26), 2292–2302.
Mitrovica, J.X., Milne, G.A., 2002. On the origin of late Holocene Sea-level highstands within equatorial ocean basins. Quat. Sci. Rev. 21 (20−22), 2179–2190.
Mitrovica, J.X., Peltier, W.R., 1991. On postglacial geoid subsidence over the equatorial oceans. J. Geophys. Res. Solid Earth 96 (B12), 20053–20071.
Moraetis, D., Mattern, F., Scharf, A., Frijia, G., Kusky, T.M., Yuan, Y., El-Hussain, I., 2018. Neogene to Quaternary uplift history along the passive margin of the northeastern Arabian Peninsula, eastern Al Hajar Mountains, Oman. Quat. Res. 90, 418–434.
Muko, S., Kawasaki, K., Sakai, K., Takasu, F., Shigesada, N., 2000. Morphological plasticity in the coral Porites sillimaniani and its adaptive significance. Bull. Mar. Sci. 66 (1), 225–239.
Murray, J.W., 1991. Ecology and Paleoecology of Benthic Foraminifera. Longman, Harlow, p. 397.
Nakada, M., Lambeck, K., 1987. Glacial rebound and relative sea-level variations: a new appraisal. Geophys. J. Int. 90 (1), 171–224.
Normand, R., Simpson, G., Herman, F., Biswas, R.H., Bahroudi, A., Schneider, B., 2019. Dating and morpho-stratigraphy of uplifted marine terraces in the Makran subduction zone (Iran). Earth Surf. Dyn. 7 (1), 321–344.
Oppenheimer, M., Glavovic, B.C., Hinkel, J., van de Wal, R., Magnan, A.K., Abd-Elgawad, A., Cai, R., Cifuentes-Jara, M., DeConto, R.M., Ghosh, T., Hay, J., Isla, F., Marzeion, B., Meyssignac, B., Sebesvari, Z., 2019. Sea level rise and implications for low-lying islands, coasts and communities. In: Pörtner, H.-O., Roberts, D.C., Masson-Delmotte, V., Zhai, P., Tignor, M., Poloczanska, E., Mintenbeck, K., Alegría, A., Nicolai, M., Okem, A., Petzold, J., Rama, B., Weyer, N.M. (Eds.), IPCC Special Report on the Ocean and Cryosphere in a Changing Climate. Cambridge University Press, Cambridge, UK and New York, NY, USA, pp. 321–445. https://doi.org/10.1017/9781009157964.006.
Oveisi, B., Lavé, J., van der Beek, P., 2007. Rates and processes of active folding evidenced by Pleistocene terraces at the central Zagros front (Iran). In: Thrust Belts and Foreland Basins: From Fold Kinematics to Hydrocarbon Systems. Springer, Berlin Heidelberg, pp. 267–287.
Paillard, D., 2010. Climate and the orbital parameters of the Earth. Compt. Rendus Geosci. 342 (4–5), 273–285. https://doi.org/10.1016/j.crte.2009.12.006.
Parker, J.H., Gischler, E., Eisenhauer, A., 2012. Biodiversity of foraminifera from late Pleistocene to Holocene coral reefs, South Sinai, Egypt. Mar. Micropaleontol. 86, 59–75.
Pavlopoulos, K., Moraetis, D., Foumelis, M., Scharf, A., Mattern, F., Forman, S., Papageorgiou, E., de Gelder, G., 2023. Uplift dynamics of the obducted northeastern continental margin of the Arabian Peninsula, Sultanate of Oman. Geochem. Geophys. Geosyst. 24 (11), e2023GC011054. https://doi.org/10.1029/2023GC011054.
Pedoja, K., Husson, L., Regard, V., Cobbold, P.R., Ostanciaux, E., Johnson, M.E., Delcaillau, B., 2011. Relative Sea-level fall since the last interglacial stage: are coasts uplifting worldwide? Earth Sci. Rev. 108 (1–2), 1–15. https://doi.org/10.1016/j.earscirev.2011.05.002.
Pedoja, K., Husson, L., Johnson, M.E., Melnick, D., Witt, C., Pochat, S., Garestier, F., 2014. Coastal staircase sequences reflecting sea-level oscillations and tectonic uplift during the Quaternary and Neogene. Earth Sci. Rev. 132, 13–38. https://doi.org/10.1016/j.earscirev.2014.01.007.
Peltier, W.R., 1999. Global sea level rise and glacial isostatic adjustment. Glob. Planet. Chang. 20 (2–3), 93–123.
Peters, T., Battashy, M.A., Bläsi, H., Hauser, M., Immenhauser, A., Moser, L., Rajhi, A.A., 2000. Geological Map of SUR and AL ASHKHARAH. Expanatory Notes. Sultanate of Oman, Ministry of Commerce and Industry, Directorate General of Minerals.
Petraglia, M.D., Parton, A., Groucutt, H.S., Alsharekh, A., 2015. Green Arabia: Human prehistory at the crossroads of continents. Quat. Int. 382, 1–7.
Philippe, M., 1998. Les Échinides Miocènes du bassin du Rhône: révision systématique. Première partie. Publ. du musée des Confluences 36 (1), 3–241.
Pirazzoli, P.A., 1993. Global sea-level changes and their measurement. Glob. Planet. Chang. 8 (3), 135–148.
Pirazzoli, P.A., Montaggioni, L.F., 1986. Late Holocene Sea-Level changes in the Northwest Tuamotu Islands, French Polynesia1. Quat. Res. 25 (3), 350–368.
Pirazzoli, P.A., Reyss, J.L., Fontugne, M., Haghipour, A., Hilgers, A., Kasper, H.U., Radtke, U., 2004. Quaternary coral-reef terraces from Kish and Qeshm Islands, Persian Gulf: new radiometric ages and tectonic implications. Quat. Int. 120 (1), 15–27.
Preusser, F., Radies, D., Driehorst, F., Matter, A., 2005. Late Quaternary history of the coastal Wahiba sands, Sultanate of Oman. J. Quat. Sci.: Publ. Quat. Res. Assoc. 20 (4), 395–405.
Reyss, J.L., Pirazzoli, P.A., Haghipour, A., Hatte, C., Fontugne, M., 1999. Quaternary marine terraces and tectonic uplift rates on the south coast of Iran. Geol. Soc. Lond. Spec. Publ. 146 (1), 225–237.
Rohling, E.J., Hibbert, F.D., Grant, K.M., Galaasen, E.V., Irvalı, N., Kleiven, H.F., Yu, J., 2019. Asynchronous Antarctic and Greenland ice-volume contributions to the last interglacial sea-level highstand. Nat. Commun. 10 (1), 5040. https://doi.org/10.1038/s41467-019-12874-3.
Rose, J.I., Usik, V.I., Marks, A.E., Hilbert, Y.H., Galletti, C.S., Parton, A., Roberts, R.G., 2011. The Nubian complex of Dhofar, Oman: an African middle stone age industry in southern Arabia. PLoS One 6 (11), e28239.
Rovere, A., Dutton, A., 2021. PALSEA: 13 years of ice-sheet and sea-level science. Past Global Changes Magazine 29 (1), 18–20. https://doi.org/10.22498/pages.29.1.18. https://pastglobalchanges.org/publications/pages-magazines/pages-magazine/13246.
Rovere, A., Raymo, M.E., Vacchi, M., Lorscheid, T., Stocchi, P., Gomez-Pujol, L., Hearty, P.J., 2016a. The analysis of last Interglacial (MIS 5e) relative sea-level indicators: Reconstructing Sea-level in a warmer world. Earth Sci. Rev. 159, 404–427.
Rovere, A., Stocchi, P., Vacchi, M., 2016b. Eustatic and relative sea level changes. Curr. Clim. Chang. Rep. 2, 221–231.
Rovere, A., Ryan, D.D., Vacchi, M., Dutton, A., Simms, A., Murray-Wallace, C., 2022. Introducing WALIS, the World Atlas of last Interglacial Shorelines Version 1.0. In EGU General Assembly Conference Abstracts (pp. EGU22-2489).
Rovere, A., Ryan, D.D., Vacchi, M., Dutton, A., Simms, A.R., Murray-Wallace, C.V., 2023. The world atlas of last interglacial shorelines (version 1.0). Earth Syst. Sci. Data 15 (1), 1–23.
Saber, M., Kantoush, S.A., Sumi, T., Ogiso, Y., Alharrasi, T., Koshiba, T., Hadidi, A., 2022. Integrated Study of Flash Floods in Wadi Basins considering Sedimentation and climate Change: An International Collaboration Project. Wadi Flash Floods: Challenges and Advanced Approaches for disaster Risk Reduction, 401-422. In: Sumi, T., et al. (Eds.), Wadi Flash Floods, Natural Disaster Science and Mitigation Engineering: DPRI Reports. Springer. https://doi.org/10.1007/978-981-16-2904-4_15.
Sana, A., Chitrakar, P., Baawain, M., Al-Mamun, A., 2023. Baseline Measurements of Waves and Currents along the Coast of Oman. J. Marine Sci. Eng. 11 (9), 1711. https://doi.org/10.3390/jmse11091711.
Shannon, C.E., Weaver, W., 1949. The Mathematical Theory of Communication. The University of llinois Press, Urbana, p. 117.
Small, C., Nicholls, R.J., 2003. A global analysis of human settlement in coastal zones. J. Coast. Res. 584-599. https://doi.org/10.2307/4299200.
Spada, G., 2017. Glacial isostatic adjustment and contemporary sea level rise: an overview. Integr. Study Mean Sea Level Comp. 155–187.
Steffen, H., Wu, P., 2011. Glacial isostatic adjustment in Fennoscandia—a review of data and modeling. J. Geodyn. 52 (3–4), 169–204.
Törnqvist, T.E., Rosenheim, B.E., Hu, P., Fernandez, A.B., 2015. Radiocarbon dating and calibration. Handbook Sea-Level Res. 347–360.
Williams, A.H., Walkden, G.M., 2002. Late Quaternary highstand deposits of the southern Arabian Gulf: a record of sea-level and climate change. Geol. Soc. Lond. Spec. Publ. 195 (1), 371–386.
Wyns, R., Le Métour, J., Roger, J., Chevrel, S., 1992. Geological Map of Sur 1:250,000, Sheet NF 40–08, Explanatory Notes. Ministry of Petroleum and Minerals, Directorate General of Minerals, Muscat, Oman, p. 80.
Yokoyama, Y., Purcell, A., 2021. On the geophysical processes impacting palaeo-sea-level observations. Geosci. Lett. 8, 13. https://doi.org/10.1186/s40562-021-00184-w.